Approximate Subspace-Based Iterative Adaptive Approach for Fast Two-Dimensional Spectral Estimation

Weize Sun, Hing Cheung So, *Senior Member, IEEE*, Yuan Chen, Long-Ting Huang, and Lei Huang, *Member, IEEE*

***Abstract*—In this paper, we devise a new approach for fast implementation of two-dimensional (2-D) iterative adaptive approach (IAA) using single or multiple snapshots. Our underlying idea is to apply the subspace methodology in this nonparametric technique by performing the IAA on the dominant singular vectors extracted from the singular value decomposition (SVD) or higher-order SVD of the multidimensional observations. In doing so, 2-D IAA is approximately realized by multiple steps of 1-D IAA, implying that computational attractiveness is achieved particularly for large data size, number of grid points and/or snapshot number. Algorithms based on matrix and tensor operations are developed, and their implementation complexities are analyzed. Computer simulations are also included to compare the proposed approach with the state-of-the-art techniques in terms of resolution probability, spectral estimation performance and computational requirement.**

***Index Terms*—Iterative adaptive approach, multidimensional harmonic retrieval, spectral estimation, tensor algebra, subspace method, array processing, MIMO radar.**

I. Introduction

MULTIDIMENSIONAL spectral estimation has been one of the fundamental problems in a diversity of important fields in science and engineering such as multiple-input multiple output (MIMO) radar [1], geometry-based channel modeling in wireless communication systems [2], and nuclear magnetic resonance spectroscopy [3]. Generally speaking, spectral estimators can be divided into parametric and nonparametric approaches [4]. Parametric-based algorithms assume that the received signal satisfies a generating model with known functional form. According to the assumed model, it is able to construct the optimal estimators such as maximum likelihood and nonlinear least squares methods, but their computational complexity is extremely large for higher-dimensional signals. On the other hand, the subspace methodology, which is usually based on multiple signal classification (MUSIC) [3], estimation of signal parameters via rotational invariance techniques (ESPRIT) [5], [6], multidimensional folding (MDF) [7], [8] or principal-singular-vector utilization for modal analysis (PUMA) [9], [10] can provide accurate estimates at a lower computational cost provided that the signal source number is known *a priori* or estimated by the MDL [11] or its variants [12], [13]. Their underlying principle is to separate the data into signal and noise subspaces via eigenvalue decomposition of the sample covariance matrix or singular value decomposition (SVD) of the raw data matrix, and the parameters of interest are then extracted from the corresponding eigenvectors, singular vectors, eigenvalues or singular values. It is worth noting that the tensor-based approach [6], [8], which exploits higher-order SVD (HOSVD), can attain a higher estimation accuracy than that of the matrix-based schemes for observations with tensorial structure. However, a major drawback of the parametric techniques is that performance degradation will be resulted when there is a mismatch between the assumed and actual signal models.

The nonparametric approach has the key advantage that no assumptions are made about the observations. In particular, there is no need to know the number of components in the data. A conventional representative is the discrete Fourier transform (DFT) but its resolution is fundamentally limited by the available observation length. To improve the resolvability, Capon [14] method and amplitude and phase estimator (APES) [15], as well as their fast implemenations [16], which basically require multiple snapshots to estimate the sample covariance matrices, have been developed. In case of single snapshot, a spatial smoothing step is needed at the expense of data length reduction. Recently, the nonlinear spectral estimation problem is reformulated as a linear model whose coefficients, representing amplitudes at different frequencies on a fine grid, are updated iteratively according to weighted least squares (WLS), and this technique is called iterative adaptive approach (IAA) [17]. Although IAA will only converge locally, it avoids spatial smoothing and thus is superior to the Capon method and APES in terms of resolution performance. It is worth pointing out that for highly-sparse data models, its sparity-aware variants including IAA-sparse learning via iterative minimization (IAA-SLIM) [18] and IAA-sparse iterative covariance-based estimation (IAA-SPICE) [19] can be employed, and they are able to retrieve the small amount of dominant peaks and simultaneously suppress the ripples. In fact, IAA has been applied in

Manuscript received July 04, 2013; revised January 07, 2014 and April 14, 2014; accepted April 14, 2014. Date of publication April 24, 2014; date of current version May 20, 2014. The associate editor coordinating the review of this manuscript and approving it for publication was Prof. Eduard Axel Jorswieck. This work was supported by a grant from the NSFC/RGC Joint Research Scheme sponsored by the Research Grants Council of Hong Kong and the Nature Science Foundation of China (Project No.: N_CityU 104/11, 61110229/61161160564), and in part supported by the National Natural Science Foundation of China under Grants 61222106.

W. Sun, H. C. So, Y. Chen, and L.-T. Huang are with Department of Electronic Engineering, City University of Hong Kong, Hong Kong, China.

Lei Huang is with the Department of Electronic and Information Engineering, Harbin Institute of Technology Shenzhen Graduate School, Shenzhen 518055, China (e-mail: dr.lei.huang@ieee.org).

Color versions of one or more of the figures in this paper are available online at http://ieeexplore.ieee.org.

Digital Object Identifier 10.1109/TSP.2014.2320460

many applications such as fundamental frequency estimation [20], MIMO radar imaging [21], channel prediction [22], blood velocity estimation [23] and synthetic aperture radar (SAR) imaging [24]. Furthermore, IAA has been extended to produce the spectra for multidimensional signals with nonuniform sampling in [25]. Nevertheless, the IAA methodology has significant computational requirement particularly when the size of data, number of grid points, snapshot number or signal dimension is high. To reduce the complexity, fast IAA implementations such as IAA with Gohberg-Semencul factorization [26], [27] and superfast quasi-Newton IAA [24], [28], which are referred to as IAA-GS and IAA-QN, respectively, have been proposed. However, it is still computationally demanding for them to handle multidimensional signals and/or data of a large size. In this work, we contribute to the development of a subspace-based IAA for two-dimensional (2-D) observations especially when the data and/or grid size are large.

The rest of the paper is organized as follows. In Section II, we first formulate the 2-D spectral estimation problem and then review the 2-D IAA [26], [27]. The subspace-based IAA for 2-D single-snapshot data is devised in Section III. By employing SVD on the 2-D measurements, dominant singular vectors are obtained to which 1-D IAA is applied. In doing so, complexity reduction is achieved by converting the 2-D operations to 1-D ones. The 2-D spectrum is finally produced via properly combining the 1-D spectra. We then extend the development to the scenario of multiple snapshots in Section IV. A matrix-based scheme is first proposed, followed by a tensor-based solution derived from tensor algebra and HOSVD. In Section V, simulation results are included to evaluate the performance of the subspace approach by comparing with the IAA-GS [26], IAA-QN [24] and MUSIC [3] algorithm in terms of resolution probability, spectral line estimation accuracy and computational complexity. Finally, conclusions are drawn in Section VI.

Notation: Scalars, vectors, matrices and tensors are denoted by italic, bold lower-case, bold upper-case and bold calligraphic symbols, respectively. The noise-free $\mathbf{A}$ is denoted by $\widetilde{\mathbf{A}}$ while $^T, ^H, ^*, ^{-1}$ and † represent the transpose, conjugate transpose, complex conjugate, inverse, and pseudoinverse, respectively. The $\mathbf{I}_i$ symbolizes the $i \times i$ identity matrix. The $\mathrm{diag}(\mathbf{a})$ denotes a diagonal matrix with vector $\mathbf{a}$ as the main diagonal, and the element-wise magnitude of $\mathbf{A}$ is $|\mathbf{A}|$. Furthermore, we write $\mathbf{A} := \mathbf{B}$ to define $\mathbf{A}$ as $\mathbf{B}$ while vec is the vectorization operator, and $\otimes$ and $\odot$ represent the Kronecker product and Khatri-Rao matrix product, respectively. Regarding tensor operations, the rth unfolding of $\boldsymbol{\mathcal{A}} \in \mathbb{C}^{M_1 \times M_2 \times \cdots \times M_R}$ is written as $[\boldsymbol{\mathcal{A}}]_{(r)} \in \mathbb{C}^{M_r \times (M_1 M_2 \cdots M_{r-1} M_{r+1} \cdots M_R)}$ where the order of the columns is chosen according to [29]. The r-mode product of tensor $\boldsymbol{\mathcal{A}}$ along the rth dimension and matrix $\mathbf{U} \in \mathbb{C}^{N_r \times M_r}$ is expressed as $\boldsymbol{\mathcal{B}} = \boldsymbol{\mathcal{A}} \times_r \mathbf{U} \in \mathbb{C}^{M_1 \times M_2 \times \cdots \times M_{r-1} \times N_r \times M_{r+1} \times \cdots \times M_R}$ where $[\boldsymbol{\mathcal{B}}]_{(r)} = \mathbf{U}[\boldsymbol{\mathcal{A}}]_{(r)}$. Note that $\boldsymbol{\mathcal{B}}$ can be interpreted as multiplying all r-mode vectors of $\boldsymbol{\mathcal{A}}$ by $\mathbf{U}$. The symbol $\sqcup$ represents the concatenation operator where $\boldsymbol{\mathcal{A}} = \boldsymbol{\mathcal{A}}_1 \sqcup_r \boldsymbol{\mathcal{A}}_2$ is obtained by stacking $\boldsymbol{\mathcal{A}}_2 \in \mathbb{C}^{M_1 \times M_2 \times \cdots \times M_{r-1} \times L_2 \times M_{r+1} \times \cdots \times M_R}$ to the end of $\boldsymbol{\mathcal{A}}_1 \in \mathbb{C}^{M_1 \times M_2 \times \cdots \times M_{r-1} \times L_1 \times M_{r+1} \times \cdots \times M_R}$ along the rth dimension.

II. Problem Formulation and Review of IAA

In this section, we first formulate the 2-D spectral estimation problem with single snapshot and then extend it to the multiple-snapshot case, followed by a review of their 2-D IAA solutions.

A. Problem Formulation

Without loss of generality, we consider the harmonic retrieval model with $M_1 \times M_2$ samples where $M_1 \geq M_2$. The observed 2-D signal, denoted by $\mathbf{Y} \in \mathbb{C}^{M_1 \times M_2}$, is [1], [6]:

$$\mathbf{Y} = \mathbf{X} + \mathbf{Q} \tag{1}$$

where

$$\mathbf{X} = \mathbf{B}_{\omega_1} \mathrm{diag}(\mathbf{c}) \mathbf{B}_{\omega_2} \tag{2}$$

$$\mathbf{B}_{\omega_r} = [\, \mathbf{a}_{M_r}(\omega_{r,1}) \quad \mathbf{a}_{M_r}(\omega_{r,2}) \quad \cdots \quad \mathbf{a}_{M_r}(\omega_{r,F}) \,] \tag{3}$$

$$\mathbf{a}_{M_r}(\omega) = [\, 1 \quad e^{j\omega} \quad \cdots \quad e^{j(M_r-1)\omega} \,]^T \tag{4}$$

$$\mathbf{c} = [\, c_1 \quad c_2 \quad \cdots \quad c_F \,]^T \tag{5}$$

for $r = 1, 2$, and $\omega_{r,f} \in (-\pi, \pi)$ represents the fth frequency in the rth dimension while c_f is the complex-valued amplitude of the fth component, $f = 1, 2, \ldots, F$, where F is the number of harmonics. The $\mathbf{X}$ is the signal of interest and $\mathbf{Q}$ is the noise matrix whose entries are uncorrelated zero-mean Gaussian distributed variables with variance σ^2. The $\{\omega_{r,f}\}, \mathbf{c}$ and σ^2 are unknown constants. Given $\mathbf{Y}$, the task is to find the F 2-D frequencies $\boldsymbol{\omega}_1 = [\, \omega_{1,1} \quad \omega_{1,2} \quad \cdots \quad \omega_{1,F} \,]$ and $\boldsymbol{\omega}_2 = [\, \omega_{2,1} \quad \omega_{2,2} \quad \cdots \quad \omega_{2,F} \,]$.

Although frequency estimation is a nonlinear problem, it can be converted into a linear model by writing $\mathbf{X}$ as [26], [27]:

$$\mathbf{X} = \mathbf{A}_{M_1} \widetilde{\mathbf{Z}} \mathbf{A}_{M_2}^T \tag{6}$$

where $\widetilde{\mathbf{Z}} \in \mathbb{C}^{K_1 \times K_2}$ and $\mathbf{A}_{M_r} = [\, \mathbf{a}_{M_r}(\omega_0) \quad \mathbf{a}_{M_r}(\omega_1) \quad \cdots \quad \mathbf{a}_{M_r}(\omega_{K_r-1}) \,], r = 1, 2$, with $\omega_{k_r} = 2\pi k_r / K_r, k_r = 0, 1, \ldots, K_r - 1$, representing the grid points. It is easy to see that (6) is valid when K_1 and K_2 are sufficiently large such that $\{\omega_{r,f}\}$ align exactly with the F nonzero points in the $K_1 \times K_2$ grid. That is, the (k_1, k_2) entry of $\widetilde{\mathbf{Z}}$, denoted by $\tilde{z}_{k_1,k_2}$, is

$$\tilde{z}_{k_1,k_2} = \begin{cases} c_f, & \text{if } \omega_{k_1} = \omega_{1,f} \quad \text{and} \quad \omega_{k_2} = \omega_{2,f} \\ 0, & \text{otherwise} \end{cases} \tag{7}$$

Based on (6), the task of spectral estimation can be interpreted as finding the F dominant peaks of the magnitude-squared spectrum, denoted by $\mathbf{P}$:

$$\mathbf{P} = |\mathbf{Z}|^2, \quad p_{k_1,k_2} = |z_{k_1,k_2}|^2 \tag{8}$$

from the noisy $\mathbf{Y}$.

When multiple snapshots are available, we can extend (1) as

$$\mathbf{Y}(t) = \mathbf{X}(t) + \mathbf{Q}(t), \quad t = 1, 2, \ldots, T \tag{9}$$

where t is the snapshot index and T is the number of snapshots. Following (2) and (6), $\mathbf{X}(t)$ has the form of:

$$\mathbf{X}(t) = \mathbf{B}_{\omega_1} \mathrm{diag}(\mathbf{c}(t)) \mathbf{B}_{\omega_2}^T \tag{10}$$

and

$$\mathbf{X}(t) = \mathbf{A}_{M_1} \widetilde{\mathbf{Z}}(t) \mathbf{A}_{M_2}^T \tag{11}$$

where the 2-D frequencies are fixed while the amplitudes vary among different snapshots. Although $\{\widetilde{\mathbf{Z}}(t)\}$ are distinct, the locations of their magnitude peaks are equal. In the presence

of noise, $\mathbf{Z}(t)$ is computed from $\mathbf{Y}(t)$, and we follow [27] to determine the magnitude-squared spectrum:

$$\mathbf{P} = \sum_{t=1}^{T} |\mathbf{Z}(t)|^2 \tag{12}$$

where each $\mathbf{Z}(t)$ has the same weighting. Again, the frequency estimates are found by locating the F dominant peaks of $\mathbf{P}$.

B. Iterative Adaptive Approach

According to [26], the procedure for IAA using single-snapshot 2-D data is reviewed as follows. With the use of (6), the received data matrix of (1) can be written as:

$$\mathbf{Y} = \mathbf{X} + \mathbf{Q} \approx \mathbf{A}_{M_1}\mathbf{Z}\mathbf{A}_{M_2}^T \tag{13}$$

where $\mathbf{Z}$ is the spectral estimate of $\mathbf{Y}$. Note that $\mathbf{Z} \neq \widetilde{\mathbf{Z}}$ because it contains both signal and noise components, and when DFT is employed to retrieve $\mathbf{Z}$, the approximation in (13) becomes exact. Vectorizing both sides of (13) yields:

$$\mathbf{y} \approx \mathbf{A}_{M_1,M_2}\mathbf{z} \tag{14}$$

where $\mathbf{y} = \mathrm{vec}(\mathbf{Y}), \mathbf{z} = \mathrm{vec}(\mathbf{Z})$ and $\mathbf{A}_{M_1,M_2} = \mathbf{A}_{M_1} \otimes \mathbf{A}_{M_2}$ whose columns are $\mathbf{a}_{M_1,M_2}(k_1,k_2) = \mathbf{a}_{M_1}(\omega_{k_1}) \otimes \mathbf{a}_{M_2}(\omega_{k_2})$, $k_r = 0, 1, \ldots, K_r - 1$. Conceptually, the 2-D IAA solves the (k_1, k_2) entry of $\mathbf{Z}$ by minimizing the WLS cost function:

$$\|\mathbf{y} - \mathbf{a}_{M_1,M_2}(k_1,k_2)z_{k_1,k_2}\|^2_{\mathbf{Q}^{-1}_{M_1,M_2}(k_1,k_2)} \tag{15}$$

for $k_1 = 0, 1, \ldots, K_1-1, k_2 = 0, 1, \ldots, K_2-1$, and the inverse of the weighting matrix has the form:

$$\begin{aligned}&\mathbf{Q}_{M_1,M_2}(k_1,k_2)\\ &\quad = \mathbf{R}_{M_1,M_2} - p_{k_1,k_2}\mathbf{a}_{M_1,M_2}(k_1,k_2)\mathbf{a}_{M_1,M_2}(k_1,k_2)^H\end{aligned} \tag{16}$$

where

$$\begin{aligned}\mathbf{R}_{M_1,M_2} = \mathbf{A}_{M_1,M_2}\Phi(\mathbf{z})\Phi(\mathbf{z})^H\mathbf{A}^H_{M_1,M_2},\\ \Phi(\mathbf{z}) = \mathrm{diag}(\mathbf{z})\end{aligned} \tag{17}$$

In practice, z_{k_1,k_2} is computed in an iterative manner:

$$\begin{aligned}z_{k_1,k_2} &= \frac{\mathbf{a}_{M_1,M_2}(k_1,k_2)^H\mathbf{Q}^{-1}_{M_1,M_2}(k_1,k_2)\mathbf{y}}{\mathbf{a}_{M_1,M_2}(k_1,k_2)^H\mathbf{Q}^{-1}_{M_1,M_2}(k_1,k_2)\mathbf{a}_{M_1,M_2}(k_1,k_2)}\\ &= \frac{\mathbf{a}_{M_1,M_2}(k_1,k_2)^H\mathbf{R}^{-1}_{M_1,M_2}\mathbf{y}}{\mathbf{a}_{M_1,M_2}(k_1,k_2)^H\mathbf{R}^{-1}_{M_1,M_2}\mathbf{a}_{M_1,M_2}(k_1,k_2)}\end{aligned} \tag{18}$$

The entries of $\mathbf{Z}$ can be initialized by 2-D DFT with zero padding and we update $\mathbf{R}_{M_1,M_2}$ and $\mathbf{Z}$ according to (17) and (18) alternately until a stopping criterion is reached.

Extending (15) to the multiple-snapshot case of $T > 1$, the WLS cost function for estimating the elements of $\mathbf{Z}(t)$, denoted by $z_{k_1,k_2,t}$, is [27]:

$$\|\mathbf{y}_t - \mathbf{a}_{M_1,M_2}(k_1,k_2)z_{k_1,k_2,t}\|^2_{\mathbf{Q}^{-1}_{M_1,M_2}(k_1,k_2)} \tag{19}$$

where $\mathbf{y}_t = \mathrm{vec}(\mathbf{Y}(t)), t = 1, 2, \ldots, T$. Analogous to (17), the matrix $\mathbf{R}_{M_1,M_2}$ can be calculated as

$$\mathbf{R}_{M_1,M_2} = \mathbf{A}_{M_1,M_2}\left(\sum_{t=1}^{T}\Phi(\mathbf{z}_t)\Phi(\mathbf{z}_t)^H\right)\mathbf{A}^H_{M_1,M_2} \tag{20}$$

where $\Phi(\mathbf{z}_t) = \mathrm{diag}(\mathrm{vec}(\mathbf{Z}(t)))$. That is, the summation of all magnitude-squared spectra is used instead of a single one. Here, $z_{k_1,k_2,t}$ is iteratively updated according to (18) with the substitution of $\mathbf{y} = \mathbf{y}_t$. Upon convergence, the spectrum is determined using (12).

At each iteration, the major complexity order for directly updating $z_{k_1,k_2,t}$ is $\mathcal{O}(2M^2KT) + \mathcal{O}(MKT) + \mathcal{O}(\iota_{\mathrm{inv}}M^3)$ where $M = M_1M_2, K = K_1K_2$ and $\iota_{\mathrm{inv}} \geq 1$ is associated with the method for the matrix inverse computation. Typically, very large values of K_1 and K_2 are needed to achieve high resolution performance. Moreover, in applications such as SAR imaging [24], the observation sizes, namely, M_1 and M_2, are also large, leading to a big $\mathbf{R}_{M_1,M_2}$. Both result in significant computational load. To reduce the standard IAA computational requirement, techniques such as IAA-GS [26] and IAA-QN [24] have been suggested. For single snapshot, the complexity orders of the former and latter are $\mathcal{O}(3K\log K)+\mathcal{O}(M^2M_2)+\mathcal{O}(M_2M\log M)$ and $\mathcal{O}(3K\log K) + \mathcal{O}(1.5M_1^2L_2^3) + \mathcal{O}(M_1^3L_2) + \mathcal{O}(4M_1^2L_2) + \mathcal{O}(3M_1^2L_2\log(2M_1)) + \mathcal{O}(2M_1^3\log M) + \mathcal{O}(20M_1^2L_2\log(4M_1L_2))$, respectively, where $L_2 < M_2$ is a user-defined parameter. Since the term $\mathcal{O}(\iota_{\mathrm{inv}}M^3)$ is not involved, complexity reduction will be achieved when M is large. However, the term $\mathcal{O}(3K\log K)$ becomes dominant when $K \gg M$, and even these fast algorithms will be computationally demanding. The same problem also applies to the multiple-snapshot scenario. For example, the complexity order of the IAA-GS for $T \geq 1$ is generalized as $\mathcal{O}((T+2)K\log K) + \mathcal{O}(M^2M_2) + \mathcal{O}(TM_2M\log M)$. It is seen that when the number of snapshots is large, the computational burden will significantly increase because of $\mathcal{O}((T+2)K\log K) + \mathcal{O}(TM_2M\log M)$. In this work, we propose to utilize the subspace methodology to achieve fast IAA computation particularly for $K \gg 1$ and/or $T \gg 1$.

III. Estimation With Single Snapshot

In this section, we first show that the 2-D DFT of a 2-D matrix can be computed using 1-D DFT of its singular vectors. Employing the same idea, we exploit 1-D IAA for approximating the 2-D IAA implementation in order to achieve fast computation.

Using SVD, the data matrix of (1) is:

$$\mathbf{Y} = \mathbf{U}\mathbf{\Lambda}\mathbf{V}^H = \mathbf{U}_{1s}\mathbf{\Lambda}_s\mathbf{V}_s^H + \mathbf{U}_{1n}\mathbf{\Lambda}_n\mathbf{V}_n^H \tag{21}$$

where $\mathbf{U}_{1s} = [\,\mathbf{u}_{1,1} \quad \mathbf{u}_{1,2} \quad \cdots \quad \mathbf{u}_{1,F_s}\,]$ and $\mathbf{U}_{2s} := \mathbf{V}_s^* = [\,\mathbf{u}_{2,1} \quad \mathbf{u}_{2,2} \quad \cdots \quad \mathbf{u}_{2,F_s}\,]$ are the F_s dominant left and right singular vectors while $\mathbf{\Lambda}_s = \mathrm{diag}([\,\lambda_1 \quad \lambda_2 \quad \cdots \quad \lambda_{F_s}\,])$ contains the corresponding singular values such that $\lambda_1 \geq \lambda_2 \geq \cdots \geq \lambda_{F_s}$, and they are the signal subspace components. On the other hand, $\mathbf{U}_{1n}, \mathbf{\Lambda}_n$ and $\mathbf{V}_n$ belong to the noise subspace. When the number of harmonics, namely, F, is known, we set

$F_s = \min\{F, M_2\}$. Otherwise, $F_s = M_2$ is assigned, indicating that all singular vectors are used. Then (21) can be approximated as:

$$\mathbf{Y} \approx \sum_{f=1}^{F_s} \lambda_f \mathbf{u}_{1,f}\mathbf{u}_{2,f}^T = \sum_{f=1}^{F_s} \lambda_f \mathbf{Y}_f, \quad \mathbf{Y}_f = \mathbf{u}_{1,f}\mathbf{u}_{2,f}^T \tag{22}$$

Note that the approximation becomes exact when $F_s = M_2$ or $F_s = \min\{F, M_2\}$ in the absence of noise. Equation (22) indicates that $\mathbf{Y}$ can be determined by a linear combination of $\{\mathbf{Y}_f\}$ and each $\mathbf{Y}_f$ is the outer product of two vectors, namely, $\mathbf{u}_{1,f}$ and $\mathbf{u}_{2,f}$. Analogous to the association of $\mathbf{Y}$ and $\mathbf{Z}$ in (13), we write:

$$\mathbf{Y}_f \approx \mathbf{A}_{M_1}\mathbf{Z}_f\mathbf{A}_{M_2}^T \tag{23}$$

$$\mathbf{u}_{r,f} \approx \mathbf{A}_{M_r}\mathbf{z}_{r,f}, \quad r = 1, 2 \tag{24}$$

where $\mathbf{Z}_f$ and $\mathbf{z}_{r,f}$ denote the spectral representations of $\mathbf{Y}_f$ and $\mathbf{u}_{r,f}$, respectively. Combining (13) and (23)–(24) yields

$$\mathbf{Z} \approx \sum_{f=1}^{F_s} \lambda_f \mathbf{Z}_f \approx \sum_{f=1}^{F_s} \lambda_f \mathbf{z}_{1,f}\mathbf{z}_{2,f}^T, \quad \mathbf{Z}_f \approx \mathbf{z}_{1,f}\mathbf{z}_{2,f}^T \tag{25}$$

Note that the rank of $\mathbf{Z}_f$ is approximately equal to 1, and our main idea of achieving computational efficiency is to find $\mathbf{z}_{1,f}$ and $\mathbf{z}_{2,f}$ instead of $\mathbf{Z}$, which will be detailed shortly. Now we first prove that $\mathbf{Z}_f = \mathbf{z}_{1,f}\mathbf{z}_{2,f}^T$ holds exactly in (25) when $\mathbf{Z}$ corresponds to Fourier transform with $F_s = M_2$. Let $\mathbf{Z} = \mathbf{Z}^{\mathrm{F}} \in \mathbb{C}^{K_1 \times K_2}$ and $\mathbf{z}_{r,f} = \mathbf{z}_{r,f}^{\mathrm{F}} \in \mathbb{C}^{K_r \times 1}$ be the zero-padded 2-D DFT and 1-D DFT of $\mathbf{Y}$ and $\mathbf{u}_{r,f}$, scaled by $1/K$ and $1/K_r$, respectively. According to DFT definition, (13) and (23)–(24) will hold exactly and thus there is no approximation in (25).

Let $\mathbf{y}_f = \mathrm{vec}(\mathbf{Y}_f) = \mathbf{u}_{2,f} \otimes \mathbf{u}_{1,f}$. With the use of (13)–(15) and (23), the (k_1, k_2) entry of $\mathbf{Z}_f$, denoted by $z_{k_1,k_2,f}$, is computed according to:

$$\min_{z_{k_1,k_2,f}} \|\mathbf{y}_f - \mathbf{a}_{M_1,M_2}(k_1,k_2) z_{k_1,k_2,f}\|^2_{\mathbf{Q}^{-1}_{M_1,M_2,f}(k_1,k_2)} \tag{26}$$

where the weighting matrix $\mathbf{Q}^{-1}_{M_1,M_2,f}(k_1,k_2)$ is distinct for each $\mathbf{Y}_f, f = 1, 2, \ldots, F_s$. The $z_{k_1,k_2,f}$ is iteratively updated according to (18) with substitution of $\mathbf{y} = \mathbf{y}_f$ and $\mathbf{R}_{M_1,M_2} = \mathbf{R}_{M_1,M_2,f}$ where $\mathbf{R}_{M_1,M_2,f}$ has the form of:

$$\mathbf{R}_{M_1,M_2,f} = \mathbf{A}_{M_1,M_2}\Phi(\mathbf{z}_f)\Phi(\mathbf{z}_f)^H\mathbf{A}^H_{M_1,M_2} \tag{27}$$

Employing DFT for the algorithm initialization, we have $\mathbf{z}_f = \mathrm{vec}(\mathbf{Z}_f) = \mathbf{z}_{2,f} \otimes \mathbf{z}_{1,f}$ at the beginning. According to (24)–(25), $\mathbf{z}_{r,f}$ is the 1-D spectral estimate of $\mathbf{u}_{r,f}, r = 1, 2$, and the rank-1 approximation of $\mathbf{Z}_f$ is constructed from $\mathbf{z}_{1,f}$ and $\mathbf{z}_{2,f}$. Applying $\mathbf{Z}_f \approx \mathbf{z}_{1,f}\mathbf{z}_{2,f}^T$, which implies $\Phi(\mathbf{z}_f) \approx \Phi(\mathbf{z}_{2,f}) \otimes \Phi(\mathbf{z}_{1,f})$, (27) can then be expressed as:

$$\begin{aligned}\mathbf{R}_{M_1,M_2,f} &\approx (\mathbf{A}_{M_2} \otimes \mathbf{A}_{M_1})(\Phi(\mathbf{z}_{2,f}) \otimes \Phi(\mathbf{z}_{1,f})) \\ &\quad \times (\Phi(\mathbf{z}_{2,f})^H \otimes \Phi(\mathbf{z}_{1,f})^H)(\mathbf{A}_{M_2} \otimes \mathbf{A}_{M_1})^H \\ &= \mathbf{R}_{M_2,f} \otimes \mathbf{R}_{M_1,f}\end{aligned} \tag{28}$$

where

$$\mathbf{R}_{M_r,f} = \mathbf{A}_{M_r}\Phi(\mathbf{z}_{r,f})\Phi(\mathbf{z}_{r,f})^H\mathbf{A}^H_{M_r} \tag{29}$$

It is worth mentioning that although our development here assumes a sinusoidal signal, it can be seen that (21)–(29) hold for any signal models with $F_s = M_2$.

Based on (28), and recalling $\mathbf{y}_f = \mathbf{u}_{2,f} \otimes \mathbf{u}_{1,f}$, the update of $z_{k_1,k_2,f}$ can be separated into two components:

$$b_{r,f,k_r} = \frac{\mathbf{a}_{M_r}(k_r)^H(\mathbf{R}_{M_r,f})^{-1}\mathbf{u}_{r,f}}{\mathbf{a}_{M_r}(k_r)^H(\mathbf{R}_{M_r,f})^{-1}\mathbf{a}_{M_r}(k_r)}, \quad r = 1, 2 \tag{30}$$

where

$$z_{k_1,k_2,f} = b_{1,f,k_r}b_{2,f,k_r} \quad \text{or} \quad \mathbf{Z}_f = \mathbf{b}_{1,f}\mathbf{b}_{2,f}^T \tag{31}$$

Here, $\mathbf{b}_{r,f} \in \mathbb{C}^{K_r \times 1}$ contains the elements $\{b_{r,f,k_r}\}, r = 1, 2$. Instead of computing $z_{k_1,k_2,f}$ directly, we employ (30) for spectral estimation. In doing so, computing the inverse of $\mathbf{R}_{M_1,M_2,f} \in \mathbb{C}^{M \times M}$ is replaced by inverting $\mathbf{R}_{M_1,f} \in \mathbb{C}^{M_1 \times M_1}$ and $\mathbf{R}_{M_2,f} \in \mathbb{C}^{M_2 \times M_2}$, which results in significant complexity reduction. According to (25) and (31), the last issue we need to address is to estimate $\{z_{k_1,k_2,f}\}$ from $\mathbf{b}_{1,f}$ and $\mathbf{b}_{2,f}$, which are equal to $\mathbf{z}_{1,f}$ and $\mathbf{z}_{2,f}$, up to unknown scalars, respectively.

To make the remaining estimation procedure clearer, we include an index i in $\mathbf{z}_{r,f}^{(i)}$ and $\mathbf{b}_{r,f}^{(i)}, r = 1, 2$, to represent their values at the ith iteration as follows. Without loss of generality, $\mathbf{z}_{1,f}^{(i+1)}$ is first estimated with the use of $\mathbf{z}_{2,f}^{(i)}$, $\mathbf{b}_{1,f}^{(i)}$ and $\mathbf{b}_{2,f}^{(i)}$. Assuming that the difference between $\mathbf{z}_{r,f}^{(i)}$ and $\mathbf{z}_{r,f}^{(i+1)}$ is sufficiently small, we have:

$$\mathbf{z}_{1,f}^{(i+1)}\left(\mathbf{z}_{2,f}^{(i)}\right)^T \approx \mathbf{Z}_f = \mathbf{b}_{1,f}^{(i)}\left(\mathbf{b}_{2,f}^{(i)}\right)^T \tag{32}$$

Solving (32) in least squares (LS) simply yields:

$$\mathbf{z}_{1,f}^{(i+1)} \approx \left(\mathbf{z}_{2,f}^{(i)}\right)^{\dagger}\mathbf{b}_{2,f}^{(i)}\mathbf{b}_{1,f}^{(i)} \tag{33}$$

In a similar manner, $\mathbf{z}_{2,f}^{(i+1)}$ is then computed as:

$$\mathbf{z}_{2,f}^{(i+1)} \approx \left(\mathbf{z}_{1,f}^{(i+1)}\right)^{\dagger}\mathbf{b}_{1,f}^{(i+1)}\mathbf{b}_{2,f}^{(i)} \tag{34}$$

Upon convergence of the successive updates of (33) and (34) with i_{iter} iterations, we employ (25) to construct the approximate version of $\mathbf{Z}$. The estimation procedure of the proposed method, which is referred to as subspace-IAA, is summarized in Table I.

Finally, we analyze the complexity of the subspace-IAA. First, the SVD of $\mathbf{Y}$ has an order of $\mathcal{O}(k_t F M_1 M_2)$, where k_t is a constant depending on the design of the algorithm [30]. In each iteration, the inverse of $R_{M_r,f}$ for $r = 1, 2, f = 1, 2, \ldots, F_s$, requires a complexity order of $\mathcal{O}(\iota_{\mathrm{inv}} M_r^3)$. Second, the computational load of $\mathbf{b}_{r,f}$ and $\mathbf{z}_{r,f}$, according to [27], is $\mathcal{O}(2K_rM_r^2) + \mathcal{O}(K_rM_r) + \mathcal{O}(3K_r)$ for each iteration. Therefore, the overall complexity is $\mathcal{O}(k_tFM_1M_2) + i_{\mathrm{iter}}F_s\sum_{r=1}^{2}[\mathcal{O}(\iota_{\mathrm{inv}}M_r^3) + \mathcal{O}(2K_rM_r^2) + \mathcal{O}(K_r(M_r+3))]$. Note that when the data sizes, M_1 and M_2, are very large, further computation reduction techniques [26], [27] can be employed together with the procedure in Table I. For large M and/or K, the dominant complexity terms in the IAA-GS and IAA-QN are $\mathcal{O}(3K \log K)$ and $\mathcal{O}(M^2M_2)$. While our proposal does not contain these terms because normally $K_r \ll K$ and

TABLE I
ALGORITHM FOR SUBSPACE-IAA

(i) Perform SVD on $\mathbf{Y}$ to obtain $\{\mathbf{u}_{r,f}\}$ and λ_f, $r = 1, 2$, $f = 1, 2, \cdots, F_s$, in (21)
for each f
(ii) Compute $\mathbf{z}_{1,f}^{(0)}$ and $\mathbf{z}_{2,f}^{(0)}$ from DFT of $\mathbf{u}_{1,f}$ and $\mathbf{u}_{2,f}$ with scaling factors $1/K_1$ and $1/K_2$, respectively
(iii) Given $\mathbf{z}_{2,f}^{(i)}$, obtain $(\mathbf{R}_{M_2,f}^{(i)})^{-1}$ and $\mathbf{b}_{2,f}^{(i)}$ according to (29) and (30)
(iv) Given $\mathbf{z}_{1,f}^{(i)}$ and $\mathbf{b}_{2,f}^{(i)}$, compute $(\mathbf{R}_{M_1,f}^{(i)})^{-1}$, and then update $\mathbf{z}_{1,f}^{(i+1)}$ using (29) and (33)
(v) Given $\mathbf{z}_{1,f}^{(i+1)}$, update $(\mathbf{R}_{M_1,f}^{(i+1)})^{-1}$ and compute $\mathbf{b}_{1,f}^{(i+1)}$ using (30), $\mathbf{z}_{2,f}^{(i+1)}$ is then updated using (29) and (34)
(vi) Do (iii)–(v) for i_{iter} times
end for
(vii) Compute $\mathbf{Z}$ according to (25)

$M_r \ll M$. That is to say, the latter will be more computationally attractive because most of the complexity terms are only a function of M_1 or M_2 and/or K_1 or K_2, but not their products.

IV. EXTENSION TO MULTIPLE SNAPSHOTS

In this section, we will extend the subspace-IAA for handling multiple-snapshot data. A matrix-based algorithm is first developed first, followed by a tensor method.

A. Matrix-Based Approach

According to (9)–(11), we stack $\{\mathbf{Y}(t)\}$ into a matrix, denoted by $\mathbf{Y}_m$:

$$\mathbf{Y}_m = [\,\mathbf{Y}(1) \quad \mathbf{Y}(2) \quad \cdots \quad \mathbf{Y}(T)\,] = \mathbf{X}_m + \mathbf{Q}_m \tag{35}$$

where

$$\mathbf{X}_m = \mathbf{B}_{\omega_1}(\mathbf{C} \odot \mathbf{B}_{\omega_2})^T \tag{36}$$

$$\mathbf{C} = [\,\mathbf{c}(1) \quad \mathbf{c}(2) \quad \cdots \quad \mathbf{c}(T)\,] \tag{37}$$

The $\mathbf{X}_m$ and $\mathbf{Q}_m$ are defined accordingly. Analogous to (21)–(22), performing SVD on (35) gives

$$\mathbf{Y}_m \approx \mathbf{U}_{1s}\mathbf{\Lambda}_s\mathbf{U}_{2s}^T = \sum_{f=1}^{F_s}\lambda_f\mathbf{u}_{1,f}\mathbf{u}_{2m,f}^T = \sum_{f=1}^{F_s}\lambda_f\mathbf{Y}_{m,f} \tag{38}$$

where $\mathbf{u}_{1,f}$ and $\mathbf{u}_{2m,f}, f = 1, 2, \ldots, F_s$, are the fth columns of $\mathbf{U}_{1s}$ and $\mathbf{U}_{2s}$, respectively, which are the dominant singular vectors but now $F_s = \min\{F, M_1, M_2T\}$. Comparing (36) and (38), we deduce that in the noise-free case, $\mathrm{span}(\widetilde{\mathbf{U}}_{2s}) \subseteq \mathrm{span}(\mathbf{C} \odot \mathbf{B}_{\omega_2})$, and thus

$$\widetilde{\mathbf{U}}_{2s} = (\mathbf{C} \odot \mathbf{B}_{\omega_2})\mathbf{\Omega} \tag{39}$$

where $\mathbf{\Omega} \in \mathbb{C}^{F_s \times F_s}$ is an unknown nonsingular matrix. In the presence of noise, $\mathbf{u}_{2m,f}$ can then be approximated as

$$\begin{aligned}\mathbf{u}_{2m,f} &\approx (\mathbf{C} \odot \mathbf{B}_{\omega_2})\mathbf{w}_f \\ &:= [\,\mathbf{u}_{2,f}(1)^T \quad \mathbf{u}_{2,f}(2)^T \quad \cdots \quad \mathbf{u}_{2,f}(T)^T\,]^T\end{aligned} \tag{40}$$

where $\mathbf{w}_f$ is the fth column of $\mathbf{\Omega}$. That is, $\mathbf{u}_{2m,f}$ is a 1-D signal with T snapshots and $\mathbf{u}_{2,f}(t) = (\mathbf{c}(t) \odot \mathbf{B}_\mu)\mathbf{w}_f$ corresponds to the tth snapshot data. Similar to (25), we obtain:

$$\begin{aligned}\mathbf{Z}_m &= [\,\mathbf{Z}(1) \quad \mathbf{Z}(2) \quad \cdots \quad \mathbf{Z}(T)\,] \approx \sum_{f=1}^{F_s}\lambda_f\mathbf{Z}_{m,f} \\ &= \sum_{f=1}^{F_s}\lambda_f\,[\,\mathbf{Z}_f(1) \quad \mathbf{Z}_f(2) \quad \cdots \quad \mathbf{Z}_f(T)\,]\end{aligned} \tag{41}$$

and

$$\mathbf{Z}_f(t) = \mathbf{z}_{1,f}\mathbf{z}_{2,f}(t)^T \tag{42}$$

where $\mathbf{Z}_m, \mathbf{z}_{1,f}$ and $\mathbf{z}_{2,f}(t)$ are the spectral representations of $\mathbf{Y}_m, \mathbf{u}_{1,f}$ and $\mathbf{u}_{2,f}(t)$, respectively. Following the same steps as in (26)–(34) and introducing the iteration index $i, \mathbf{z}_{1,f}$ and $\mathbf{z}_{2,f}(t)$ are updated using

$$\mathbf{z}_{1,f}^{(i+1)} \approx \left(\mathbf{z}_{2m,f}^{(i)}\right)^\dagger \mathbf{b}_{2m,f}^{(i)}\mathbf{b}_{1,f}^{(i)} \tag{43}$$

$$\begin{aligned}\mathbf{z}_{2m,f}^{(i+1)} &\approx \left(\mathbf{z}_{1,f}^{(i+1)}\right)^\dagger \mathbf{b}_{1,f}^{(i+1)}\mathbf{b}_{2m,f}^{(i)} \\ &= \left[\,\mathbf{z}_{2,f}^{(i+1)}(1)^T \quad \mathbf{z}_{2,f}^{(i+1)}(2)^T \quad \cdots \quad \mathbf{z}_{2,f}^{(i+1)}(T)^T\right]^T\end{aligned} \tag{44}$$

$$\mathbf{b}_{2m,f} = [\,\mathbf{b}_{2,f}(1)^T \quad \mathbf{b}_{2,f}(2)^T \quad \cdots \quad \mathbf{b}_{2,f}(T)^T\,]^T \tag{45}$$

where $\mathbf{R}_{M_1,f}$ and $\mathbf{b}_{1,f}$ are similar to (29) and (30), respectively. On the other hand, the k_2th element of $\mathbf{b}_{2,f}(t)$, namely, $b_{2,f,k_2}(t)$ is computed according to (30) with the substitution of $r = 2$ and $\mathbf{u}_{2,f} = \mathbf{u}_{2,f}(t), k_2 = 1, 2, \ldots, K_2$, and $\mathbf{R}_{M_2,f}$ is now:

$$\mathbf{R}_{M_2,f} = \mathbf{A}_{M_2}\left(\sum_1^T \Phi(\mathbf{z}_{r,f}(t))\Phi(\mathbf{z}_{r,f}(t))^H\right)\mathbf{A}_{M_2}^H \tag{46}$$

because there are T snapshots and we follow the definition in (20). After a stopping criterion is reached, $\mathbf{Z}_{m,f}$ can be calculated from $\mathbf{z}_{1,f}$ and $\mathbf{z}_{2m,f}$ as that in (25). We then determine $\mathbf{Z}_m$ using (41) and finally, the spectrum is given by (12).

Following the estimation steps in the single-snapshot case, the major complexity order of the multiple-snapshot approach is $\mathcal{O}(k_t F M_1 M_2 T) + i_{\mathrm{iter}} F_s[\mathcal{O}(\sum_{r=1}^2 \iota_{\mathrm{inv}} M_r^3) + \mathcal{O}(2K_1M_1^2) + \mathcal{O}(K_1(M_1+3)) + \mathcal{O}(2K_2M_2^2T) + \mathcal{O}(K_2(M_2+3)T)]$. We again see the computational attractiveness of our proposal over the IAA-GS and IAA-QN.

Note that in joint direction-of-departure and direction-of-arrival estimation in MIMO radar [1], it is assumed that $T \gg M_1$, then the term $\mathcal{O}(2K_2M_2^2T) + \mathcal{O}(K_2(M_2+3)T)$, which is due to the update of $b_{2,f,k_2}(t)$ of (45) will dominate and make the proposed algorithm less computationally efficient. To address this issue, we assume that T can be factorized as $T = T_1T_2$ and construct a modified form of $\mathbf{Y}_m$:

$$\mathbf{Y}_m = \begin{bmatrix} \mathbf{Y}(1) & \mathbf{Y}(2) & \cdots & \mathbf{Y}(T_1) \\ \mathbf{Y}(T_1+1) & \mathbf{Y}(T_1+2) & \cdots & \mathbf{Y}(2T_1) \\ \vdots & \vdots & \ddots & \vdots \\ \mathbf{Y}((T_2-1)T_1+1) & \mathbf{Y}((T_2-1)T_1+2) & \cdots & \mathbf{Y}(T_1T_2) \end{bmatrix} \tag{47}$$

The estimation procedure is almost the same but now the singular vectors in both dimensions should be considered. Following the same steps, a similar approach as in (43)–(45) can be devised, but the complexity order now becomes $\mathcal{O}(k_t F M_1 M_2 T) + i_{\text{iter}} F_s \sum_{r=1}^{2} [\mathcal{O}(\iota_{\text{inv}} M_r^3) + \mathcal{O}(2K_r M_r^2 T_r) + \mathcal{O}(K_r(M_r+3)T_r)]$.

B. Tensor-Based Approach

Apart from employing matrix operations, we investigate the tensor approach by considering the multiple-snapshot data as 3-D data. This is easily done by stacking the finite snapshots $\{\mathbf{Y}(t)\}$ along the third dimension:

$$\begin{aligned}\boldsymbol{\mathcal{Y}} &= \mathbf{Y}(1) \sqcup_3 \mathbf{Y}(2) \sqcup_3 \cdots \sqcup_3 \mathbf{Y}(T) \\ &= \boldsymbol{\mathcal{X}} + \boldsymbol{\mathcal{Q}}\end{aligned} \tag{48}$$

where $\boldsymbol{\mathcal{X}}$ and $\boldsymbol{\mathcal{Q}}$ are the corresponding signal and noise tensors.

Applying the truncated HOSVD on $\boldsymbol{\mathcal{Y}}$, we can write [29]:

$$\boldsymbol{\mathcal{Y}} \approx \boldsymbol{\mathcal{S}}_s \times_1 \mathbf{U}_{1s} \times_2 \mathbf{U}_{2s} \times_3 \mathbf{U}_{3s} \tag{49}$$

which can be considered as an extension of (21)–(22) to tensor data. The $\boldsymbol{\mathcal{S}}_s \in \mathbb{C}^{F_1 \times F_2 \times F_T}$ is the signal core ordered tensor, while $\mathbf{U}_{rs} = [\,\mathbf{u}_{r,1} \quad \mathbf{u}_{r,2} \quad \cdots \quad \mathbf{u}_{r,F_r}\,] \in \mathbb{C}^{M_r \times F_r}, r = 1, 2$, and $\mathbf{U}_{3s} \in \mathbb{C}^{T \times F_T}$ are the signal subspace components. When the number of sources is known *a priori*, the values of F_r and F_T are $F_r = \min\{F, M_r, MT/M_r\}$ and $F_T = \min\{F, T, M\}$. Otherwise, $F_r = \min\{M_r, MT/M_r\}$ and $F_T = \min\{T, M\}$. In practice, they are computed from the truncated SVD of $[\boldsymbol{\mathcal{Y}}]_{(r)}^T$ [29]:

$$[\boldsymbol{\mathcal{Y}}]_{(r)}^T = \mathbf{U}_r \mathbf{S}_r \mathbf{V}_r^H = \mathbf{U}_{rs} \mathbf{S}_{rs} \mathbf{V}_{rs}^H + \mathbf{U}_{rn} \mathbf{S}_{rn} \mathbf{V}_{rn}^H \tag{50}$$

According to [6], the signal component in (49) is

$$\boldsymbol{\mathcal{Y}}_s = \boldsymbol{\mathcal{S}}_s \times_1 \mathbf{U}_{1s} \times_2 \mathbf{U}_{2s} \in \mathbb{C}^{M_1 \times M_2 \times F_T} \tag{51}$$

We further define $\boldsymbol{\mathcal{Z}} \in \mathbb{C}^{K_1 \times K_2 \times T}$ and $\boldsymbol{\mathcal{Z}}_s \in \mathbb{C}^{K_1 \times K_2 \times F_T}$ as the spectral representations of $\boldsymbol{\mathcal{Y}}$ and $\boldsymbol{\mathcal{Y}}_s$:

$$\boldsymbol{\mathcal{Y}} \approx \boldsymbol{\mathcal{Z}} \times_1 \mathbf{A}_{M_1} \times_2 \mathbf{A}_{M_2} \tag{52}$$

and

$$\boldsymbol{\mathcal{Y}}_s \approx \boldsymbol{\mathcal{Z}}_s \times_1 \mathbf{A}_{M_1} \times_2 \mathbf{A}_{M_2} \tag{53}$$

Note that (52)–(53) are in fact a tensor generalization of (13). Based on (49) and (51), we get

$$\boldsymbol{\mathcal{Z}} \approx \boldsymbol{\mathcal{Z}}_s \times_3 \mathbf{U}_{3s} \tag{54}$$

Writing

$$\boldsymbol{\mathcal{Z}} = \mathbf{Z}(1) \sqcup_3 \mathbf{Z}(2) \sqcup_3 \cdots \sqcup_3 \mathbf{Z}(T) \tag{55}$$

$$\boldsymbol{\mathcal{Z}}_s = \mathbf{Z}_s(1) \sqcup_3 \mathbf{Z}_s(2) \sqcup_3 \cdots \sqcup_3 \mathbf{Z}_s(F_T) \tag{56}$$

and noting $\mathbf{U}_{3s}^H \mathbf{U}_{3s} = \mathbf{I}_{F_T}$, we can conclude that the magnitude-squared spectra constructed from $\boldsymbol{\mathcal{Z}}$ and $\boldsymbol{\mathcal{Z}}_s$ are approximately identical, as long as they are computed from $\boldsymbol{\mathcal{Y}}$ and $\boldsymbol{\mathcal{Y}}_s$ using the same technique. Assuming that T is larger than $\min\{F, M\}$, we will determine $\boldsymbol{\mathcal{Z}}_s$ instead of finding $\boldsymbol{\mathcal{Z}}$ because the former consists of smaller snapshots.

As in Section III, there are two equivalent ways to compute the DFT of $\boldsymbol{\mathcal{Y}}_s$, denoted by $\boldsymbol{\mathcal{Z}}_s^{\text{F}}$, when $F_r = \min\{[M_r, MT/M_r]\}, r = 1, 2$. That is, we can use $\boldsymbol{\mathcal{Z}}_s^{\text{F}} = \mathbf{Z}_s^{\text{F}}(1) \sqcup_3 \mathbf{Z}_s^{\text{F}}(2) \sqcup_3 \cdots \sqcup_3 \mathbf{Z}_s^{\text{F}}(F_T)$ where each $\mathbf{Z}_s^F(f_T), f_T = 1, 2, \ldots, F_T$, corresponds to the zero-padded 2-D DFT of $\mathbf{Y}_s(f_T)$ and scaled by $1/K$ where $\boldsymbol{\mathcal{Y}}_s = \mathbf{Y}_s(1) \sqcup_3 \mathbf{Y}_s(2) \sqcup_3 \cdots \sqcup_3 \mathbf{Y}_s(F_T)$. While the alternative expression is $\boldsymbol{\mathcal{Z}}_s^{\text{F}} = \boldsymbol{\mathcal{S}}_s \times_1 \mathbf{Z}_{1s}^{\text{F}} \times_2 \mathbf{Z}_{2s}^{\text{F}}$ where $\mathbf{Z}_{rs}^{\text{F}} = [\,\mathbf{z}_{r,1}^{\text{F}} \quad \mathbf{z}_{r,2}^{\text{F}} \quad \cdots \quad \mathbf{z}_{r,F_r}^{\text{F}}\,], r = 1, 2$, and $\mathbf{z}_{r,f_r}^{\text{F}}$ is the zero-padded 1-D DFT of $\mathbf{u}_{r,f_r}$ and scaled by $1/K_r$. That is:

$$\mathbf{u}_{r,f_r} = \mathbf{A}_{M_r} \mathbf{z}_{r,f_r} \tag{57}$$

We then follow the same idea as in Section III and exploit 1-D IAA for approximating the 2-D IAA spectrum using multiple snapshots. The tensor version of (25) is now:

$$\boldsymbol{\mathcal{Z}}_s = \boldsymbol{\mathcal{S}}_s \times_1 \mathbf{Z}_{1s} \times_2 \mathbf{Z}_{2s} \tag{58}$$

where $\mathbf{Z}_{1s}$ and $\mathbf{Z}_{2s}$ will be updated in an alternating way.

Employing the DFT coefficients for the algorithm initialization, $\boldsymbol{\mathcal{Z}}$ follows (58) at the beginning. Assuming that the relation approximately holds in the subsequent iterations, we first update $\mathbf{z}_{2,f_2}$, the f_2th column of $\mathbf{Z}_{2s}$ with a fixed $\mathbf{Z}_{1s}$. The $\boldsymbol{\mathcal{Y}}_s$ of (51) can be written as

$$\begin{aligned}[\boldsymbol{\mathcal{Y}}_s]_{(2)} &= \mathbf{U}_{2s} [\boldsymbol{\mathcal{S}}_s]_{(2)} \left(\mathbf{I}_{F_T} \otimes \mathbf{U}_{1s}^T\right) = \mathbf{U}_{2s} \mathbf{U}_{1ts}^T \\ &= \sum_{f_2=1}^{F_2} \mathbf{u}_{2,f_2} \mathbf{u}_{1ts,f_2}^T = \sum_{f_2=1}^{F_2} \mathbf{Y}_{f_2}^{s(2)}\end{aligned} \tag{59}$$

where

$$\mathbf{U}_{1ts} = (\mathbf{I}_{F_T} \otimes \mathbf{U}_{1s})\, [\boldsymbol{\mathcal{S}}_s]_{(2)}^T \in \mathbb{C}^{M_1 F_T \times F_2} \tag{60}$$

$$\mathbf{u}_{1ts,f_2} = (\mathbf{I}_{F_T} \otimes \mathbf{U}_{1s})\, \mathbf{s}_{f_2}^{s(2)} \tag{61}$$

with $\mathbf{u}_{2ts,f_2}$ and $\mathbf{s}_{f_2}^{s(2)}$ being the f_2th columns of $\mathbf{U}_{2ts}$ and $[\boldsymbol{\mathcal{S}}_s]_{(2)}^T$, and

$$\mathbf{s}_{f_2}^{s(2)} = \left[\, \left(\mathbf{s}_{f_2,1}^{s(2)}\right)^T \quad \left(\mathbf{s}_{f_2,2}^{s(2)}\right)^T \quad \cdots \quad \left(\mathbf{s}_{f_2,F_T}^{s(2)}\right)^T \,\right]^T \tag{62}$$

with $\mathbf{s}_{f_2,f_T}^{s(2)} = [\,s_{1,f_2,f_T} \quad s_{2,f_2,f_T} \quad \cdots \quad s_{F_1,f_2,f_T}\,]^T$. Then $\mathbf{Y}_{f_2}^{s(2)}$ can be expressed as

$$\mathbf{Y}_{f_2}^{s(2)} = \mathbf{Y}_{f_2,1} \sqcup_2 \mathbf{Y}_{f_2,2} \sqcup_2 \cdots \sqcup_2 \mathbf{Y}_{f_2,F_T} \tag{63}$$

where

$$\mathbf{Y}_{f_2,f_T} = \mathbf{u}_{2,f_2} \left(\mathbf{s}_{f_2,f_T}^{s(2)}\right)^T \mathbf{U}_{1s}^T = \mathbf{u}_{2,f_2} \left(\mathbf{u}_{f_2,f_T}^{(1)}\right)^T \tag{64}$$

$$\mathbf{u}_{f_2,f_T}^{(1)} = \mathbf{U}_{1s} \mathbf{s}_{f_2,f_T}^{s(2)} \tag{65}$$

Instead of estimating the spectrum of $[\boldsymbol{\mathcal{Y}}_s]_{(2)}$ or $\boldsymbol{\mathcal{Y}}_s$, we can estimate that of $\mathbf{Y}_{f_2}^{s(2)}$ in (63), which is in fact an F_T-snapshot problem with F_T snapshots $\{\mathbf{Y}_{f_2,f_T}\}$ concatenated along the second dimension. This can then be solved using a similar iterative procedure as in Section IV.A.

For ease of understanding, we define the spectral representation of $\mathbf{Y}_{f_2}^{s(2)}$ as $\mathbf{Z}_{f_2} = [\,\mathbf{Z}_{f_2,1} \quad \mathbf{Z}_{f_2,2} \quad \cdots \quad \mathbf{Z}_{f_2,F_T}\,]$,

and z_{k_1,k_2,f_2,f_T} is the (k_1,k_2) entry of $\mathbf{Z}_{f_2,f_T} = \mathbf{z}_{2,f_2}(\mathbf{Z}_{1s}\mathbf{s}^{s(2)}_{f_2,f_T})^T$. The update equation of z_{k_1,k_2,f_2,f_T} is then

$$z_{k_1,k_2,f_2,f_T} = \frac{\mathbf{a}_{M_2,M_1}(k_1,k_2)^H \mathbf{R}^{-1}_{M_2,M_1,f_2}\mathbf{y}_{f_2,f_T}}{\mathbf{a}_{M_2,M_1}(k_1,k_2)^H \mathbf{R}^{-1}_{M_2,M_1,f_2}\mathbf{a}_{M_2,M_1}(k_1,k_2)} \quad (66)$$

where

$$\mathbf{R}_{M_2,M_1,f_2} = \frac{1}{F_T}\sum_{f_T=1}^{F_T} \mathbf{A}_{M_2,M_1}\Phi\left(\mathbf{z}_{f_2,f_T}\right) \times \Phi\left(\mathbf{z}_{f_2,f_T}\right)^H \mathbf{A}^H_{M_2,M_1} \quad (67)$$

$$\mathbf{z}_{f_2,f_T} = \mathrm{vec}\left(\mathbf{Z}_{f_2,f_T}\right) = \mathbf{z}_{2,f_2}\left(\mathbf{Z}_{1s}\mathbf{s}^{s(2)}_{f_2,f_T}\right)^T = \mathbf{z}^{(1)}_{f_2,f_T} \otimes \mathbf{z}_{2,f_2,f_T} \quad (68)$$

with $\mathbf{y}_{f_2,f_T} = \mathrm{vec}(\mathbf{Y}_{f_2,f_T})$ and $\mathbf{z}^{(1)}_{f_2,f_T} = \mathbf{Z}_{1s}\mathbf{s}^{s(2)}_{f_2,f_T}$. Then $\mathbf{R}_{M_2,M_1,f_2}$ can be expressed as:

$$\begin{aligned}
&\mathbf{R}_{M_2,M_1,f_2} \\
&= (\mathbf{A}_{M_1}\otimes\mathbf{A}_{M_2})\left[\frac{1}{F_T}\sum_{f_T=1}^{F_T}\Phi\left(\left(\mathbf{z}^{(1)}_{f_2,f_T}\right)\otimes\mathbf{z}_{2,f_2}\right)\right. \\
&\quad \left.\times\,\Phi\left(\left(\mathbf{z}^{(1)}_{f_2,f_T}\right)\otimes\mathbf{z}_{2,f_2}\right)^H\right](\mathbf{A}_{M_1}\otimes\mathbf{A}_{M_2})^H \\
&= \left[\frac{1}{F_T}\sum_{f_T=1}^{F_T}\left(\mathbf{A}_{M_1}\Phi\left(\mathbf{z}^{(1)}_{f_2,f_T}\right)\Phi\left(\mathbf{z}^{(1)}_{f_2,f_T}\right)\mathbf{A}^H_{M_1}\right)^H\right] \\
&\quad \otimes\left(\mathbf{A}_{M_2}\Phi(\mathbf{z}_{2,f_2})\Phi\left(\mathbf{z}_{2,f_2}\right)^H\mathbf{A}^H_{M_2}\right) \\
&= \mathbf{R}^{(1)}_{M_1,f_2}\otimes\mathbf{R}_{M_2,f_2}
\end{aligned} \quad (69)$$

where

$$\mathbf{R}^{(1)}_{M_1,f_2} := \frac{1}{F_T}\sum_{f_T=1}^{F_T}\left(\mathbf{A}_{M_1}\Phi\left(\mathbf{z}^{(1)}_{f_2,f_T}\right)\Phi\left(\mathbf{z}^{(1)}_{f_2,f_T}\right)^H\mathbf{A}^H_{M_1}\right) \in \mathbb{C}^{M_1\times M_1} \quad (70)$$

and $\mathbf{R}_{M_r,f_r}, r=1,2$, are defined similarly as in (29). Noting that $\mathbf{y}^{f_2}_{f_T} = \mathbf{u}^{(1)}_{f_2,f_T}\otimes\mathbf{u}_{2,f_2}$, (66) can be separated into two components:

$$b_{1,k_1,f_T} = \frac{\mathbf{a}_{M_1}(k_1)^H\left(\mathbf{R}^{(1)}_{M_1,f_2}\right)^{-1}\mathbf{u}^{(1)}_{f_2,f_T}}{\mathbf{a}_{M_1}(k_1)^H\left(\mathbf{R}^{(1)}_{M_1,f_2}\right)^{-1}\mathbf{a}_{M_1}(k_1)} \quad (71)$$

$$b_{2,k_2} = \frac{\mathbf{a}_{M_2}(k_2)^H\left(\mathbf{R}_{M_2,f_2}\right)^{-1}\mathbf{u}_{2,f_2}}{\mathbf{a}_{M_2}(k_2)^H\left(\mathbf{R}_{M_2,f_2}\right)^{-1}\mathbf{a}_{M_2}(k_2)} \quad (72)$$

where

$$z_{k_1,k_2,f_2,f_T} = b_{1,k_1,f_T}b_{2,k_2}, \quad \text{or} \quad \mathbf{Z}_{f_2,f_T} = \mathbf{b}_{2,f_2}\mathbf{b}^T_{1,f_2} \quad (73)$$

with $\mathbf{b}_{1,f_2} = [\,\mathbf{b}^T_{1,f_2,1}\ \mathbf{b}^T_{1,f_2,2}\ \cdots\ \mathbf{b}^T_{1,f_2,F_T}\,]^T$, and $\mathbf{b}_{1,f_2,f_T}$ and $\mathbf{b}_{2,f_2}$ are the k_1th and k_2th elements of $\mathbf{b}_{1,f_2,f_T}$ and $\mathbf{b}_{2,f_2}$, respectively. We also see that (73) is very similar to (31). Following the same steps as in (32)–(33) and including the index i in the variables to represent their values at the ith iteration, the updated $\mathbf{z}^{(i+1)}_{2,f}$ is calculated as:

$$\mathbf{z}^{(i+1)}_{2,f} \approx \left(\mathbf{z}^{(i)}_{1s,f_2}\right)^\dagger \mathbf{b}^{(i)}_{1,f_2}\mathbf{b}^{(i)}_{2,f_2} \quad (74)$$

where

$$\mathbf{z}^{(i)}_{1s,f_2} = \left(\mathbf{I}_{F_T}\otimes\mathbf{Z}^{(i)}_{1s}\right)\mathbf{s}^{s(2)}_{f_2} \quad (75)$$

For updating $\mathbf{z}_{1,f_1}$, which is the f_1th column of $\mathbf{Z}_{1s}$, we fix $\mathbf{Z}_{2s}$ and follow (59)–(73) to obtain:

$$[\boldsymbol{\mathcal{Z}}_{s,f1}]_{(1)} := [\,\mathbf{C}_{f_1,1}\ \ \mathbf{C}_{f_1,2}\ \ \cdots\ \ \mathbf{C}_{f_1,f_T}\,] \quad (76)$$

$$\mathbf{C}_{f_1,f_T} = \mathbf{c}_{1,f_1}\mathbf{c}^T_{2,f_1} \quad (77)$$

$$\mathbf{c}_{2,f_1} = [\,\mathbf{c}^T_{2,f_1,1}\ \ \mathbf{c}^T_{2,f_1,2}\ \ \cdots\ \ \mathbf{c}^T_{2,f_1,F_T}\,]^T \quad (78)$$

where the k_1th and k_2th elements of $\mathbf{c}_{1,f_1}$ and $\mathbf{c}_{2,f_1,f_T}$, denoted by c_{1,k_1} and c_{2,k_2}, are computed using

$$c_{1,k_1} = \frac{\mathbf{a}_{M_1}(k_1)^H\left(\mathbf{R}_{M_1,f_1}\right)^{-1}\mathbf{u}_{1,f_1}}{\mathbf{a}_{M_1}(k_1)^H\left(\mathbf{R}_{M_1,f_1}\right)^{-1}\mathbf{a}_{M_1}(k_1)} \quad (79)$$

$$c_{2,k_2} = \frac{\mathbf{a}_{M_2}(k_2)^H\left(\mathbf{R}^{(2)}_{M_2,f_1}\right)^{-1}\mathbf{u}^{(2)}_{f_1,f_T}}{\mathbf{a}_{M_2}(k_2)^H\left(\mathbf{R}^{(2)}_{M_2,f_1}\right)^{-1}\mathbf{a}_{M_2}(k_2)} \quad (80)$$

with

$$\mathbf{R}^{(2)}_{M_2,f_1} = \frac{1}{F_T}\sum_{f_T=1}^{F_T}\left(\mathbf{A}_{M_2}\Phi\left(\mathbf{z}^{(2)}_{f_1,f_T}\right)\times\Phi^H\left(\mathbf{z}^{(2)}_{f_1,f_T}\right)\mathbf{A}^H_{M_2}\right) \in \mathbb{C}^{M_2\times M_2} \quad (81)$$

$$\mathbf{u}^{(2)}_{f_1,f_T} = \mathbf{U}_{2s}\mathbf{s}^{s(1)}_{f_1,f_T} \quad (82)$$

$$\mathbf{z}^{(2)}_{f_1,f_T} = \mathbf{Z}_{2s}\mathbf{s}^{s(1)}_{f_1,f_T} \quad (83)$$

$$\mathbf{s}^{s(1)}_{f_1} = \left[\,\mathbf{s}^{s(1)^T}_{f_1,1}\ \ \mathbf{s}^{s(1)^T}_{f_1,2}\ \ \cdots\ \ \mathbf{s}^{s(1)\ T}_{f_1,F_T}\,\right]^T \quad (84)$$

$$\mathbf{s}^{s(1)}_{f_1,f_T} = [\,s_{f_1,1,f_T}\ \ s_{f_1,2,f_T}\ \ \cdots\ \ s_{f_1,F_2,f_T}\,]^T \quad (85)$$

The updated $\mathbf{z}^{(i+1)}_{1,f}$ is expressed as:

$$\mathbf{z}^{(i+1)}_{1,f} \approx \left(\mathbf{z}^{(i+1)}_{2s,f_1}\right)^\dagger \mathbf{c}^{(i)}_{2,f_1}\mathbf{c}^{(i)}_{1,f_1} \quad (86)$$

where

$$\mathbf{z}^{(i+1)}_{2s,f_1} = \left(\mathbf{I}_{F_T}\otimes\mathbf{Z}^{(i+1)}_{2s}\right)\mathbf{s}^{s(1)}_{f_1} \quad (87)$$

A few iterations between (74) and (86) are needed to calculate $\mathbf{Z}_{1s}$ and $\mathbf{Z}_{2s}$, and $\boldsymbol{\mathcal{Z}}_s$ can be retrieved from (58). However, since the (k_1,k_2,f_T) entry of $\boldsymbol{\mathcal{Z}}_{s,f_1}$ is already calculated in (76), it is more natural to compute $\boldsymbol{\mathcal{Z}}_s$ from

$$\boldsymbol{\mathcal{Z}}_s = \sum_{f_1=1}^{F_1}\boldsymbol{\mathcal{Z}}_{s,f_1} \quad (88)$$

That is, we calculate $\boldsymbol{\mathcal{Z}}_s$ by summing F_1 sub-spectra, and then the magnitude-squared spectrum is computed according to (12). The major computational complexity of the proposed algorithm is studied as follows. First, the HOSVD of $\boldsymbol{\mathcal{Y}}$ involves 3 SVDs, which is of $\mathcal{O}(3k_tFM_1M_2)$. The other steps

are very similar to the single-snapshot case, except that in each iteration, 4 matrices, $\mathbf{R}_{M_1,f_1}, \mathbf{R}_{M_2,f_2}, \mathbf{R}^{(1)}_{M_1,f_2}$ and $\mathbf{R}^{(2)}_{M_2,f_1}$, are now needed to perform inverse, leading to an order of $\mathcal{O}(2i_{\text{iter}}\sum_{r=1}^{2}(\iota_{\text{inv}}F_rM_r^3))$. Therefore the overall complexity order is $\mathcal{O}(3k_tFM_1M_2) + 2i_{\text{iter}}\sum_{r=1}^{2}[\mathcal{O}(\iota_{\text{inv}}F_rM_r^3) + \mathcal{O}(2K_rM_r^2F_rF_T) + \mathcal{O}(K_rM_rF_rF_T)]$. Comparing to the matrix-based scheme, it is expected that the tensor method is more computationally attractive when $T \gg F_T$.

V. Numerical Examples

Computer simulations have been carried out to evaluate the performance of the subspace-IAA approach by comparing with the IAA-GS [26], IAA-QN [24] and MUSIC [3] schemes. Since the IAA-GS and IAA-QN are exactly equal to the standard IAA subject to numerical errors, the results of the latter are not included. The harmonic retrieval models of (1)–(5) and (9)–(10) are considered in the single-snapshot and multiple-snapshot scenarios, respectively. The power of the vector $\mathbf{c}(t)$ is defined as $[\,\sigma_1^2(t) \quad \sigma_2^2(t) \quad \cdots \quad \sigma_F^2(t)\,]$ where $\sigma_f^2(t)$ follows a uniform distribution within [2], [3] in each independent run. All elements in the noise tensor $\boldsymbol{\mathcal{Q}}$ are zero mean white Gaussian processes with identical variances of σ^2. Different signal-to-noise ratio (SNR) conditions are obtained by properly scaling $\boldsymbol{\mathcal{Q}}$ where $\text{SNR} = |\text{vec}(\boldsymbol{\mathcal{X}})|_2^2/(MT\sigma^2)$. A maximum of $i_{\text{iter}} = 10$ iterations are used for all IAA techniques, but it might take less if the improvement between the ith and $(i+1)$th iterations, denoted by $e^{(i)}$, is less than a certain value ϵ. In our study, the error term $e^{(i)}$ is

$$e^{(i)} = \max\left\{\frac{\left\|\text{vec}\left(\mathbf{z}_{1,f_1}^{(i+1)}-\mathbf{z}_{1,f_1}^{(i)}\right)\right\|_2}{\left\|\text{vec}\left(\mathbf{z}_{1,f_1}^{(i)}\right)\right\|_2}, \frac{\left\|\text{vec}\left(\mathbf{z}_{2,f_2}^{(i+1)}-\mathbf{z}_{2,f_2}^{(i)}\right)\right\|_2}{\left\|\text{vec}\left(\mathbf{z}_{2,f_2}^{(i)}\right)\right\|_2}\right\} \tag{89}$$

for the proposed matrix-based algorithms, and

$$e^{(i)} = \frac{\left\|\text{vec}\left(\boldsymbol{\mathcal{Z}}^{(i+1)}-\boldsymbol{\mathcal{Z}}^{(i)}\right)\right\|_2}{\left\|\text{vec}\left(\boldsymbol{\mathcal{Z}}^{(i)}\right)\right\|_2} \tag{90}$$

for the IAA-GS, IAA-QN and tensor-based methods. Notice that the choice of ϵ might vary between (89) and (90), and in the tensor approach, F_1 might not be equal to F_2 and thus (90) is applied. All results are based on 1000 independent runs.

The first test investigates the 2-D single-snapshot case. The parameters of the noise-free signal are $M_1 = M_2 = 8, F = 4, \boldsymbol{\omega}_1 = [\,0.1392 \quad 0.1392 \quad -0.1392 \quad 0.6428\,]\pi$ and $\boldsymbol{\omega}_2 = [\,0.1392 \quad -0.1392 \quad 0.1392 \quad 0.6428\,]\,\pi$. The grid point parameters are $K_1 = K_2 = 100$ for all the methods, and SNR is set to be 10 dB. Figs. 1 to 4 show the peak estimation results for MUSIC, subspace-IAA, IAA-GS and IAA-QN approaches. Here, the subspace-IAA assumes that the number of tones, F, is known. When F is unknown, all singular vectors should be employed in Table I. It is found that the results of using F and all singular vectors are nearly identical, and thus the performance of the latter has not been included. For all the methods, the spectrum is first computed, and the 4 dominant peaks are extracted as the peak estimates. It is seen in Fig. 1 that the resolution ability of MUSIC approach is not as good as

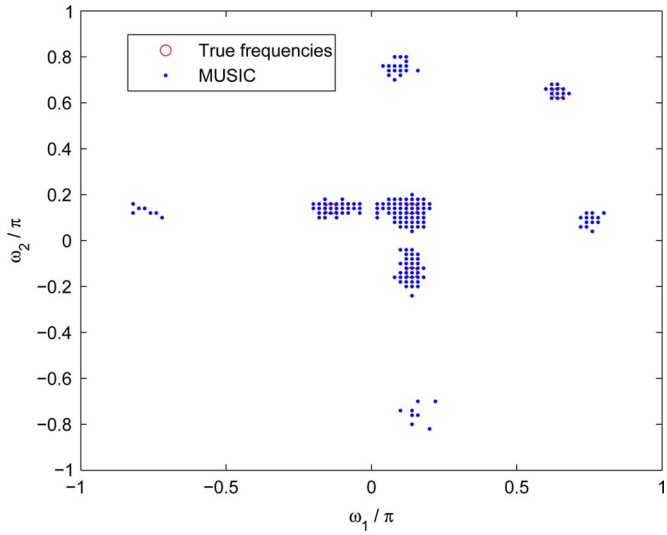

Fig. 1. Spectral line estimation performance using MUSIC.

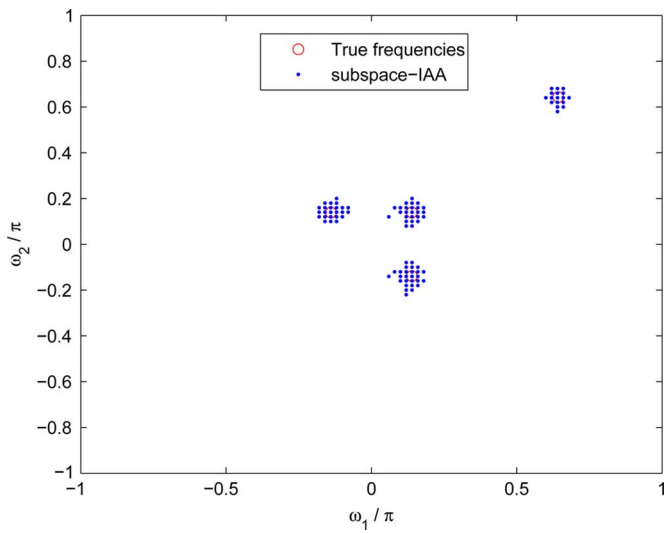

Fig. 2. Spectral line estimation performance using proposed estimator.

the others. It is due to the fact that with only single snapshot, a spatial smoothing is needed to perform prior to implementing the MUSIC, which will reduce its resolution ability. Figs. 2 to 4 show that the subspace approach performs comparably with the IAA-GS and IAA-QN. On the other hand, Fig. 5 shows the 3-D plots of their magnitude spectra in dB scale based on a typical trial. It can be seen that all the IAA-based methods successfully resolve the peaks, and the proposed algorithm has sharper main lobes but more ripples. In this single-snapshot case with $K \gg M, \mathcal{O}(3K\log K)$ is the dominant term per iteration in the IAA-GS and IAA-QN, while that of our proposal is $F_s\sum_{r=1}^{2}\mathcal{O}(2K_rM_r^2)$. The average computation times for the MUSIC, subspace-IAA, IAA-GS and IAA-QN methods are measured as 0.0841 s, 0.0113 s, 0.0470 s and 0.0489 s respectively, indicating the computational attractiveness of the proposed methodology. That is, the subspace-IAA can work about 4 times faster than the IAA-GS and IAA-QN, which agrees with the complexity analysis. Moreover, their mean square frequency errors are 0.0517, 0.0021, 0.0057 and 0.0039, respectively. Nevertheless, if we do not include the outlier

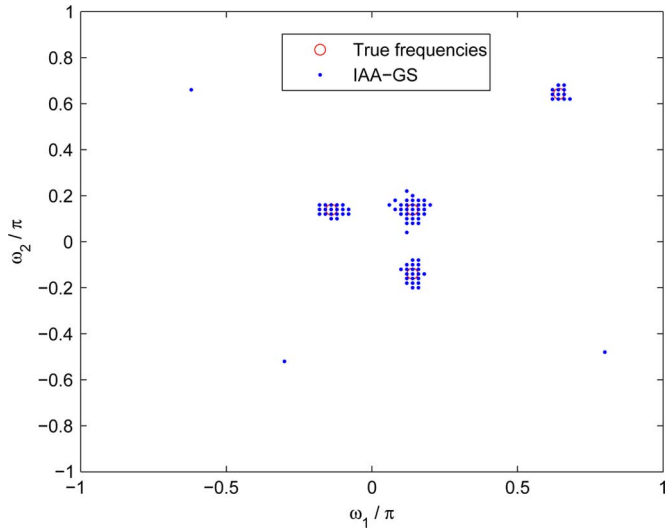

Fig. 3. Spectral line estimation performance using 2-D IAA-GS.

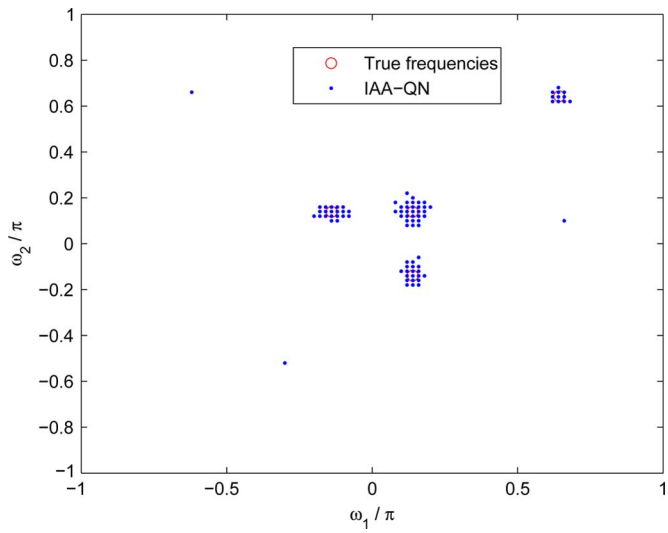

Fig. 4. Spectral line estimation performance using 2-D IAA-QN.

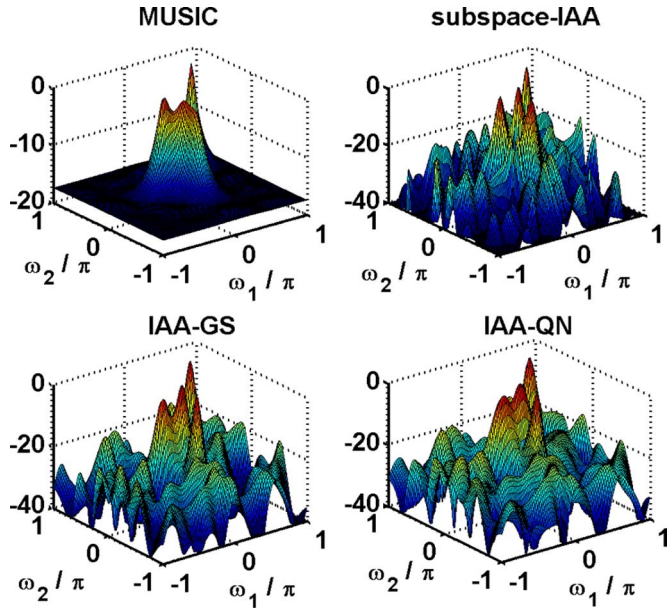

Fig. 5. 3-D magnitude spectrum at $F = 4$.

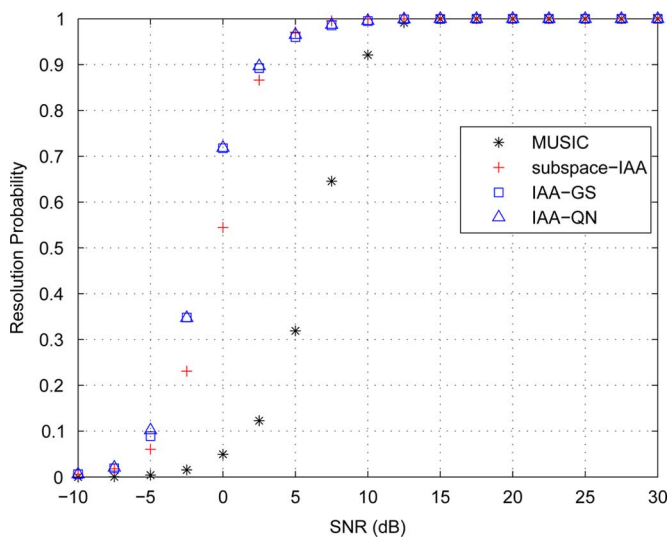

Fig. 6. Resolution probability versus SNR at $F = 4$.

points of the IAA-GS, IAA-QN and MUSIC in the calculation, the mean square error performance of all methods will be similar.

In the second test, we study the resolution probability of the estimated signals. In each independent run, we decide that the estimated $\{\hat{\omega}_{r,f}\}$ are correctly resolved if [31]

$$\text{diff}_{\hat{p}_i,p_i} + \text{diff}_{\hat{p}_j,p_j} \le \text{diff}_{p_i,p_j}$$
$$\text{diff}_{p_i,p_j} = \sqrt{\sum_{r=1}^{2} |\omega_{r,i} - \omega_{r,j}|^2} \tag{91}$$

for all $i \ne j, i, j = 1, 2, \ldots, F_s$. The parameter settings are the same as the first test, and the results of resolution probability are shown in Fig. 6. We can see that the resolution probabilities of the proposed algorithm, IAA-GS and IAA-QN are similar and they almost attain 1 when SNR $\ge$ 10 dB. We also repeat the resolution probability test for $F = 9$, where the number of sources is larger than the length of each dimension, and the frequencies are $\boldsymbol{\omega}_1 = [-0.7071 \ -0.7071 \ -0.1736 \ -0.1736 \ 0.1736 \ 0.1736 \ 0.1736 \ 0.1736 \ 0.7071]\pi$ and $\boldsymbol{\omega}_2 = [-0.7071 \ -0.1736 \ -0.1736 \ 0.1736 \ -0.7071 \ -0.1736 \ -0.1736 \ 0.5000 \ 0.5000]\pi$. The corresponding results are plotted in Fig. 7. Notice that in this case, the subspace-IAA uses all singular vectors no matter whether the number of sources is known or not. The average computation times for the MUSIC, proposed, IAA-GS and IAA-QN methods are measured as 0.0809s, 0.0218s, 0.0488s and 0.0498s, respectively.

In the third test, we consider a large data set with closely-spaced frequencies. The parameters are $M_1 = M_2 = 32, F = 15$, $\omega_1 = [0.0349 \ 0.0349 \ 0.0349 \ 0.0349 \ 0.1045 \ 0.1045 \ 0.1045 \ 0.1045 \ 0.4226 \ 0.4226 \ 0.4226 \ 0.4226 \ 0.5000 \ 0.5736 \ 0.6428]\pi$ and $\omega_2 = [0.0349 \ 0.1045 \ 0.1908 \ 0.2756 \ 0.0349 \ 0.1045 \ 0.1908 \ 0.2756 \ 0.4226 \ 0.5000 \ 0.5736 \ 0.6428 \ 0.5000 \ 0.5736 \ 0.6428]\pi$. There are two groups of frequencies where the separation between two adjacent points is less than the DFT limit. The first and second correspond to the first 8 and last 7

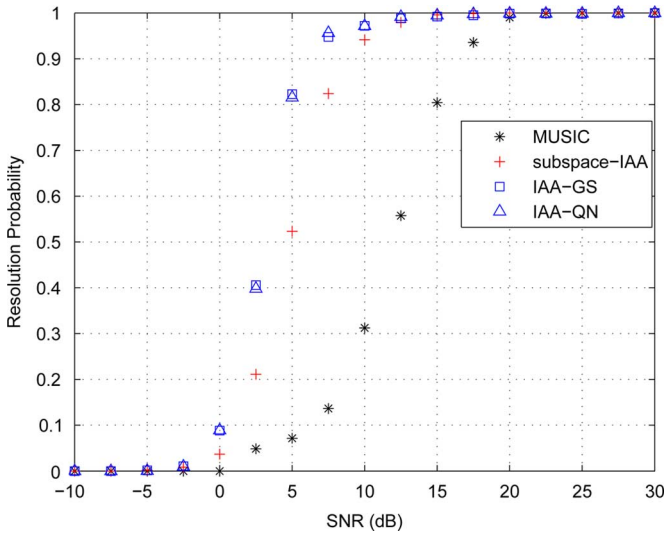

Fig. 7. Resolution probability versus SNR at $F = 9$.

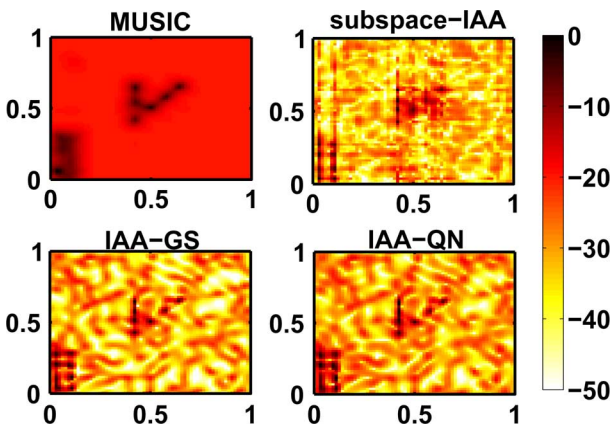

Fig. 8. Magnitude spectrum at $F = 15$.

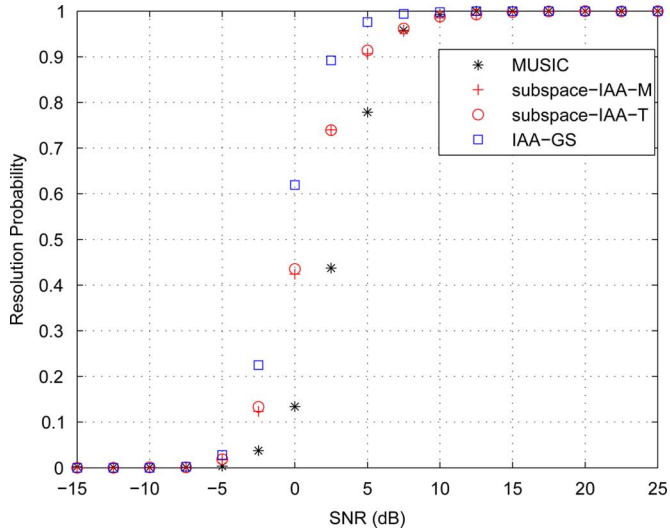

Fig. 9. Resolution probability versus SNR for 4 snapshots.

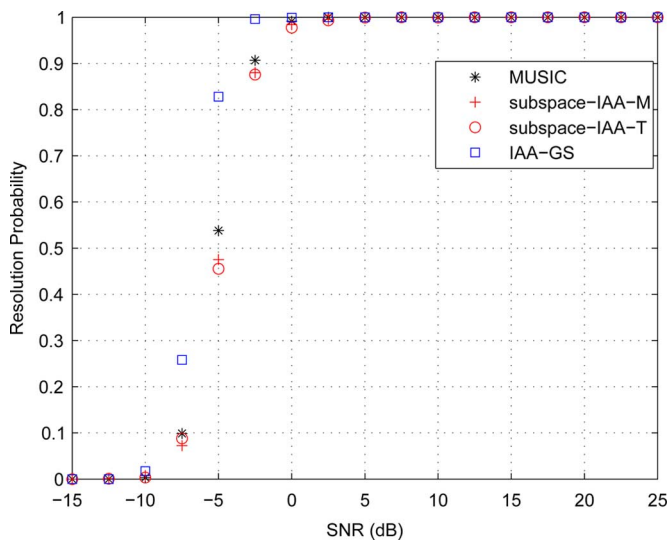

Fig. 10. Resolution probability versus SNR for 16 snapshots.

frequency pairs. The grid point parameters are $K_1 = K_2 = 128$ for all the methods, and SNR is set to be 5 dB. Note that in this setting, we have $M^2M_2 \gg K \log K$. The dominant terms in the IAA-GS and IAA-QN are now $\mathcal{O}(M^2M_2)$ and $\mathcal{O}(1.5M_1^2L_2^3)$, respectively, while that of the proposed approach is still $F_s \sum_{r=1}^{2} \mathcal{O}(2K_rM_r^2)$. The typical results in the form of single-realization 2-D contours are plotted in Fig. 8. It is observed that all IAA algorithms significantly outperform the MUSIC in resolving closely-spaced frequencies, and the proposed method has comparable sidelobe and mainlobe performance to the IAA-GS and IAA-QN. That is, the IAA can resolve most of the frequencies, with a few sources having the tendency to overlap with each other. The resolution probabilities of the MUSIC, subspace-IAA, IAA-GS and IAA-QN methods are 0, 0.889, 0.812 and 0.844, while the average computation times are measured as 1.1603 s, 0.1949 s, 1.2774 s and 0.9626 s, respectively. The subspace-IAA now works about 6 or 5 times faster than the IAA-GS or IAA-QN. We also see that the IAA-QN is a bit more computationally efficient than the IAA-GS because $L_2 < M_2$. It is expected that for larger M and/or K, the computational gain of the proposed approach is more significant. We may conclude that for single-snapshot spectral estimation, the IAA methods are superior to MUSIC, and the proposed approach can achieve almost the same performance as IAA-GS and IAA-QN when the SNR is sufficiently high, but with less computational cost.

We now examine the multiple-snapshot case. The parameter settings are the same as those in Fig. 7 except that T is now larger than 1. Figs. 9 and 10 plot the resolution probability versus SNR at $T = 4$ and $T = 16$, respectively, for the MUSIC, subspace-IAA-M, subspace-IAA-T and IAA-GS algorithms, where 'M' stands for the matrix-based method while 'T' means tensor-based, and the smoothing step follows (35) for the former. The IAA-QN is not considered for comparison from now on because its performance is very similar to that of the IAA-GS. Again, we observe that the resolution probability of the subspace-IAA is almost the same as IAA-GS for sufficiently high SNR conditions. Furthermore, when the number of snapshots increases, the difference between the IAA variants and MUSIC narrows.

Finally, the resolution probability and computational cost versus T are studied and the results are plotted in Figs. 11 and

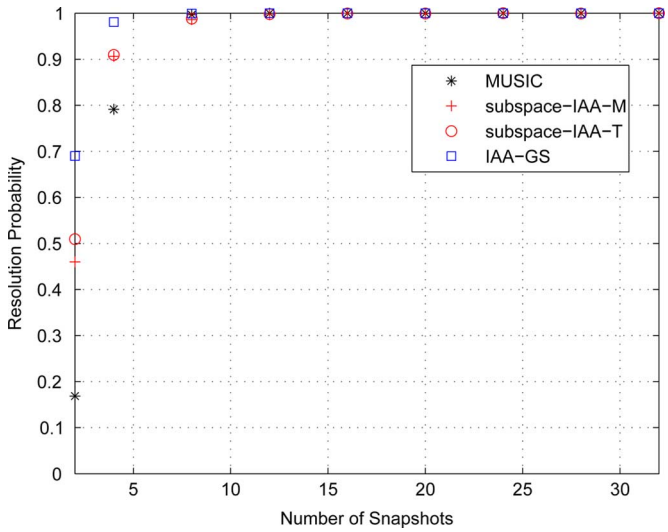

Fig. 11. Resolution probability versus T.

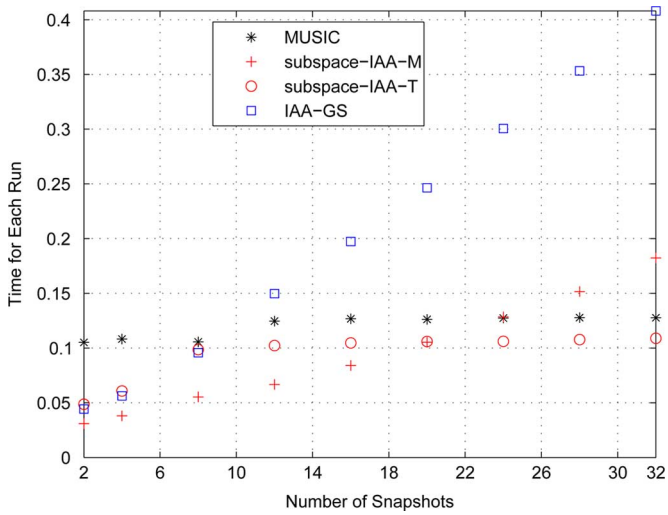

Fig. 12. Computational time versus T.

12. The parameter settings are the same as those in Fig. 10, except that SNR is set to 5 dB and T changes from 2 to 32. Fig. 11 shows that when the number of snapshots is small, the proposed methods outperform MUSIC but are worse than IAA-GS in terms of resolvability. That is, the IAA-GS achieves a resolution probability of 1 at $T \geq 8$, while the remaining methods require $T \geq 12$ snapshots to achieve the upper bound. This implies that the subspace-IAA can be inferior to the IAA-GS in small snapshot scenarios. However, when T is large enough, there is no difference. On the other hand, we can see from Fig. 12 that our proposal is faster than the IAA-GS when $T > 10$. This also aligns with our complexity analysis. It is because the dominant terms in the IAA-GS, subspace-IAA-M and subspace-IAA-T are now $\mathcal{O}((T+2)K\log K)$, $F_s\mathcal{O}(2K_2M_2^2T)$ and $2\sum_{r=1}^{2}\mathcal{O}(2K_rM_r^2F_rF_T)$, respectively. The first two increase linearly with T, while the last one is independent of T, making the tensor-based approach the most computationally efficient when $T \geq 20$. To summarize, the subspace-IAA is not superior to the existing fast IAA realizations in terms of resolution probability but the main advantage of our proposal is its computational attractiveness particularly for large M, K and/or T.

VI. Conclusion

A subspace-based approach for fast 2-D IAA using single or multiple snapshots is devised. With the use of SVD or HOSVD, the received data are decomposed into several singular vectors for each dimension. The IAA iterations are then performed on the singular vectors, which corresponds to 1-D update, instead of 2-D operations on the original measurements, and fast implementation is thus achieved. Computer simulations are included to compare the subspace approach with the IAA-GS, IAA-QN and MUSIC, demonstrating that our proposal is computationally simpler with a competitive estimation performance. Nevertheless, the subspace-IAA can be inferior to the IAA-GS in small snapshot scenarios.

Regarding directions for future research, one possibility is to exploit the sparsity structure of $\mathbf{Z}$ in our subspace algorithm development. Another one is to perform theoretical analysis of the subspace-IAA. Nevertheless, to the best of our knowledge, there is no performance analysis of the IAA available in the literature, except the local convergence [17]. Following [17], it may not be difficult to extend the local convergence proof to the 2-D IAA by constructing the corresponding cost function. However, the proposed approach is to solve the problem in the subspace domain, which introduces a big challenge in producing its analytical results, even for local convergence.

Acknowledgment

The authors would like to thank Prof. G. O. Glentis and Prof. A. Jakobsson for sharing their MATLAB code of IAA-GS and IAA-QN.

References

[1] D. Nion and N. D. Sidiropoulos, "Tensor algebra and multidimensional harmonic retrieval in signal processing for MIMO radar," *IEEE Trans. Signal Process.*, vol. 58, no. 11, pp. 5693–5705, Nov. 2010.

[2] M. Haardt, R. S. Thoma, and A. Richter, "Multidimensional high-resolution parameter estimation with applications to channel sounding," in *High-Resolution and Robust Signal Processing*, Y. Hua, A. Gershman, and Q. Chen, Eds. New York, NY, USA: Marcel Dekker, 2004, ch. 5, pp. 255–338.

[3] Y. Li, J. Razavilar, and K. J. R. Liu, "A high-resolution technique for multidimensional NMR spectroscopy," *IEEE Trans. Biomed. Eng.*, vol. 45, no. 1, pp. 78–86, Jan. 1998.

[4] P. Stoica and R. Moses, *Spectral Analysis of Signals*. Upper Saddle River, NJ, USA: Prentice-Hall, 2005.

[5] M. Haardt and J. A. Nossek, "Simultaneous Schur decomposition of several nonsymmetric matrices to achieve automatic pairing in multidimensional harmonic retrieval problems," *IEEE Trans. Signal Process.*, vol. 46, no. 1, pp. 161–169, Jan. 1998.

[6] M. Haardt, F. Roemer, and G. Del Galdo, "Higher-order SVD-based subspace estimation to improve the parameter estimation accuracy in multidimensional harmonic retrieval problems," *IEEE Trans. Signal Process.*, vol. 56, no. 7, pp. 3198–3213, Jul. 2008.

[7] J. Liu, X. Liu, and X. Ma, "Multidimensional frequency estimation with finite snapshots in the presence of identical frequencies," *IEEE Trans. Signal Process.*, vol. 55, no. 11, pp. 5179–5194, Nov. 2007.

[8] W. Sun, H. C. So, F. K. W. Chan, and L. Huang, "Tensor approach for eigenvector-based multi-dimensional harmonic retrieval," *IEEE Trans. Signal Process.*, vol. 61, no. 13, pp. 3378–3388, Jul. 2013.

[9] H. C. So, F. K. W. Chan, W. H. Lau, and C. F. Chan, "An efficient approach for two-dimensional parameter estimation of a single-tone," *IEEE Trans. Signal Process.*, vol. 58, no. 4, pp. 1999–2009, Apr. 2010.

[10] W. Sun and H. C. So, "Accurate and computationally efficient tensor-based subspace approach for multi-dimensional harmonic retrieval," *IEEE Trans. Signal Process.*, vol. 60, no. 10, pp. 5077–5088, Oct. 2012.

[11] M. Wax and T. Kailath, "Detection of signals by information theoretic criteria," *IEEE Trans. Acoust., Speech, Signal Process.*, vol. 33, no. 2, pp. 387–392, Apr. 1985.
[12] L. Huang, S. Wu, and X. Li, "Reduced-rank MDL method for source enumeration in high-resolution array processing," *IEEE Trans. Signal Process.*, vol. 55, no. 12, pp. 5658–5667, Dec. 2007.
[13] L. Huang and H. C. So, "Source enumeration via MDL criterion based on linear shrinkage estimation of noise subspace covariance matrix," *IEEE Trans. Signal Process.*, vol. 61, no. 19, pp. 4806–4821, Oct. 2013.
[14] J. Capon, "High resolution frequency-wavenumber spectrum analysis," *Proc. IEEE*, vol. 57, no. 8, pp. 1408–1418, Aug. 1969.
[15] J. Li and P. Stoica, "An adaptive filtering approach to spectral estimation and SAR imaging," *IEEE Trans. Signal Process.*, vol. 44, no. 6, pp. 1469–1484, Jun. 1996.
[16] G. O. Glentis, "A fast algorithm for APES and Capon spectral estimation," *IEEE Trans. Signal Process.*, vol. 56, no. 9, pp. 4207–4220, Sep. 2008.
[17] T. Yardibi, J. Li, P. Stoica, M. Xue, and A. B. Baggeroer, "Source localization and sensing: A nonparametric iterative adaptive approach based on weighted least squares," *IEEE Trans. Aerosp. Electron. Syst.*, vol. 46, no. 1, pp. 425–443, Jan. 2010.
[18] X. Tan, W. Roberts, J. Li, and P. Stoica, "Sparse learning via iterative minimization with application to MIMO radar imaging," *IEEE Trans. Signal Process.*, vol. 59, no. 3, pp. 1088–1101, Mar. 2011.
[19] P. Stoica, P. Babu, and J. Li, "New method of sparse parameter estimation in separable models and its use for spectral analysis of irregularly sampled data," *IEEE Trans. Signal Process.*, vol. 59, no. 1, pp. 35–47, Jan. 2011.
[20] J. R. Jensen, G. O. Glentis, M. G. Christensen, A. Jakobsson, and S. H. Jensen, "Computationally efficient IAA-based estimation of the fundamental frequency," in *Proc. 20th Eur. Signal Process. Conf. (EUSIPCO)*, Bucharest, Romania, Aug. 27–31, 2012, pp. 2163–2167.
[21] W. Roberts, P. Stoica, J. Li, T. Yardibi, and F. A. Sadjadi, "Iterative adaptive approaches to MIMO radar imaging," *IEEE J. Sel. Topics Signal Process.*, vol. 4, no. 1, pp. 5–20, Feb. 2010.
[22] D. Sun, Z. Liu, S. Ma, and K. Yi, "Channel prediction using IAA-based spectral estimation in precoded TDD-MIMO systems," *IEEE Commun. Lett.*, vol. 17, no. 4, pp. 701–704, Apr. 2013.
[23] A. Jakobsson, G. O. Glentis, and E. Gudmundson, "Computationally efficient time-recursive IAA-based blood velocity estimation," *IEEE Trans. Signal Process.*, vol. 60, no. 7, pp. 3853–3858, Jul. 2012.
[24] G. O. Glentis, K. Zhao, A. Jakobsson, and J. Li, "Non-parametric high-resolution SAR imaging," *IEEE Trans. Signal Process.*, vol. 61, no. 7, pp. 1614–1624, Apr. 2013.
[25] N. R. Butt and A. Jakobsson, "High-resolution estimation of multidimensional spectra from unevenly sampled data," in *Proc. 17th Int. Conf. Digit. Signal Process. (DSP)*, Corfu, Greece, Jul. 6–8, 2011, pp. 1–4.
[26] M. Xue, L. Xu, and J. Li, "IAA spectral estimation: Fast implementation using the Gohberg-Semencul factorization," *IEEE Trans. Signal Process.*, vol. 59, no. 7, pp. 3251–3261, Jul. 2011.
[27] G. O. Glentis and A. Jakobsson, "Efficient implementation of iterative adaptive approach spectral estimation techniques," *IEEE Trans. Signal Process.*, vol. 59, no. 9, pp. 4154–4167, Sep. 2011.
[28] G. O. Glentis and A. Jakobsson, "Superfast approximative implementation of the IAA spectral estimate," *IEEE Trans. Signal Process.*, vol. 60, no. 1, pp. 472–478, Jan. 2012.
[29] L. de Lathauwer, B. de Moor, and J. Vanderwalle, "A multilinear singular value decomposition," *SIAM J. Matrix Anal. Appl.*, vol. 21, no. 4, pp. 1253–1278, 2000.
[30] G. H. Golub and C. F. Van Loan, *Matrix Computations*. Baltimore, MD, USA: The John Hopkins Univ. Press, 1996.
[31] P. Parvazi, M. Pesavento, and A. B. Gershman, "Rooting-based harmonic retrieval using multiple shift-invariances: The complete and the incomplete sample cases," *IEEE Trans. Signal Process.*, vol. 60, no. 4, pp. 1556–1570, Apr. 2012.

Weize Sun received the B.Sc. degree from Sun Yat-Sen University, China, and the Ph.D. degree from City University of Hong Kong, both in electronic engineering, in 2009 and 2013, respectively.

His research interests include statistical signal processing, parameter estimation, tensor algebra, with particular attention to frequency estimation.

Hing Cheung So (S'90–M'95–SM'07) was born in Hong Kong. He received the B.Eng. degree from the City University of Hong Kong and the Ph.D. degree from The Chinese University of Hong Kong, both in electronic engineering, in 1990 and 1995, respectively.

From 1990 to 1991, he was an Electronic Engineer with the Research and Development Division, Everex Systems Engineering Ltd., Hong Kong. During 1995–1996, he was a Postdoctoral Fellow with The Chinese University of Hong Kong. From 1996 to 1999, he was a Research Assistant Professor with the Department of Electronic Engineering, City University of Hong Kong, where he is currently an Associate Professor. His research interests include statistical signal processing, fast and adaptive algorithms, signal detection, parameter estimation, and source localization.

Dr. So has been on the editorial boards of the *IEEE Signal Processing Magazine*, IEEE TRANSACTIONS ON SIGNAL PROCESSING, *Signal Processing*, and *Digital Signal Processing*, as well as a member of the Signal Processing Theory and Methods Technical Committee of the IEEE Signal Processing Society.

Yuan Chen received the B.S. degree in communication engineering at Shandong University, in 2010.

She is currently a Ph.D. student in the Department of Electronic Engineering at City University of Hong Kong. Her research interest is robust estimation.

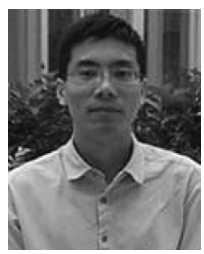

Long-Ting Huang received his M.S. degree in computer science from Wuhan Institute of Technology, China, in 2011. Currently, he is pursuing the Ph.D. degree in the Department of Electronic Engineering, City University of Hong Kong. His research interests include multidimensional frequency estimation and low-rank matrix/tensor completion.

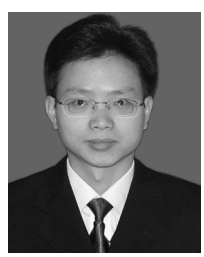

Lei Huang (M'07) was born in Guangdong, China. He received the B.Sc., M.Sc., and Ph.D. degrees in electronic engineering from Xidian University, Xian, China, in 2000, 2003, and 2005, respectively.

From 2005 to 2006, he was a Research Associate with the Department of Electrical and Computer Engineering, Duke University, Durham, NC. From 2009 to 2010, he was a Research Fellow with the Department of Electronic Engineering, City University of Hong Kong and a Research Associate with the Department of Electronic Engineering, The Chinese University of Hong Kong. Since 2011, he has been with the Department of Electronic and Information Engineering, Harbin Institute of Technology Shenzhen Graduate School, where he is currently a Professor. His research interests include spectral estimation, array signal processing, statistical signal processing, and their applications in radar and wireless communications.

Dr. Huang is currently an editorial board member of *Digital Signal Processing*.